2010-01-01

A New Green Chemistry Method Based on Plant Extracts to Synthesize Gold Nanoparticles

Milka Odemariz Montes Castillo
University of Texas at El Paso, momontes@miners.utep.edu

A NEW GREEN CHEMISTRY METHOD BASED ON PLANT EXTRACTS TO SYNTHESIZE GOLD NANOPARTICLES: MICROSCOPIC AND SPECTROSCOPIC CHARACTERIZATION

MILKA ODEMARIZ MONTES CASTILLO

Department of Chemistry

APPROVED:

Jorge L. Gardea-Torresdey, Ph.D., Chair

Geoffrey Saupe, Ph.D.

Mahesh Narayan, Ph.D.

John McClure, Ph. D.

Jose R. Peralta-Videa, Ph. D.

Patricia D. Witherspoon, Ph.D.
Dean of the Graduate School

Dedication

To my family.

A NEW GREEN CHEMISTRY METHOD BASED ON PLANT EXTRACTS TO SYNTHESIZE GOLD NANOPARTICLES

by

MILKA ODEMARIZ MONTES CASTILLO, B. S.

DISSERTATION

Presented to the Faculty of the Graduate School of

The University of Texas at El Paso

in Partial Fulfillment

of the Requirements

for the Degree of

DOCTOR OF PHILOSOPHY

Department of Chemistry

THE UNIVERSITY OF TEXAS AT EL PASO

May 2010

Acknowledgements

First and foremost, I would like to thank my advisor and mentor, Dr. Jorge L. Gardea-Torresdey, for his guidance and support through the course of my journey. He has truly inspired me to be a scientist and he has motivated me to exceed my own expectations. I will always respect him and regard him as a friend.

I would like to express my gratitude to the members of my dissertation committee: Dr. Mahesh Narayan, Dr. Geoffrey Saupe, and Dr. John McClure for their time and dedication to the success of my project; and specially to Dr. Jose R. Peralta-Videa, true mentor and friend, for helping me overcome my own limitations and for his teachings on continued and arduous work while finding inner balance.

Special thanks to Dr. Miguel Jose-Yacamán for allowing me to spend a summer as part of his electron microscopy research group at the University of Texas at San Antonio; and to the members of his group: Dr. Alvaro Mayoral, Dr. Leonard Deepak, and David Olmos for their contribution, friendship, and technical support during the microscopic characterization of my nanoparticles. I would also like to thank Dr. Domingo Ferrer, Dr. Lawrence Murr, and Sara Gaytan for HRTEM access and support. Thanks to Dr. Michael A. Grusak for allowing me to work on his research projects at the USDA/ARS Children's Nutrition Research Center at Baylor University. I learned a great deal of molecular biology and biochemical techniques during my internship with him. He has my respect and I consider him a friend.

I would also like to thank Dr. Gardea's research group, past and present. Dr. Guadalupe De la Rosa, Dr. Laura Lopez-Moreno, and Dr. Jason Parsons, for being an example to follow and for their help in my development as a scientist. My special thanks to Laura and Lupita for always encouraging me through their friendship and support. To Dr. Marcos Delgado, Dr. Gustavo Cruz-Jimenez, Dr. Elena Rodriguez, Dr. Alejandro Martinez, Dr. Sharon Mogkalaka, Dr. Kenneth Dokken, Tenoch, Alia, Yong, Rebecca, Pepe, Hiram, Christina, Fabiola, Angelica, and Kevin for being there for me. And to all the

group members that passed through during my time in Dr. Gardea's group as well as the Dudley family for its Endowed Research Professorship to him in Chemistry. Also, my deepest appreciation goes to all the faculty and staff of the Chemistry Department at UTEP for all the knowledge I acquired from them. To Dr. Michael, Dr. Mito, Dr. Dirk, Dr. Noveron, and Dr. Salvador for allowing me to spend time in their laboratories; and to Dr. Becvar, Dr. Gunn, and Dr. Lloyd for all the conversations about chemistry. Thanks to Lucema Armenta, Grace Awad, Frank Reyes, Alejandro Carrillo, and Ana Karen for making my life easier.

Special thanks to my husband, Felix Holguin for his love and support. My endless gratitude to my parents, Victoria Castillo and Manuel Montes for their love, and to my brothers (David and Alfonso), to my sisters (Vicky, Nohemy, Nidia, Clara, Silvia, Irma and Tere), and to my nephews and nieces who are my greatest inspiration to continue improving my life. Also, special thanks to all the people that demonstrated their friendship and who have touched my life in a very special way: Nancy, Ana, Fabiola, Alia, Andrew, Eric, Israel, Sergio, Tenoch, David, Karina, Molly, Bety, Vero, Pal, Roberto, and all my friends.

This work was possible thanks to the financial support of the National Science Foundation through the Bridge to the Doctorate Fellowship, the HUTEP-AGEP fellowship, the Dodson Fellowhip at UTEP, and the TA assistantship in the Chemistry Department.

This material is based upon work supported by the National Science Foundation and the Environmental Protection Agency under Cooperative Agreement Number EF 0830117. Any opinions, findings, and conclusions or recommendations expressed in this material are those of the author(s) and do not necessarily reflect the views of the National Science Foundation or the Environmental Protection Agency. This work has not been subjected to EPA review and official endorsement should not be inferred. The author also acknowledges the USDA grant number 2008-38422-19138**,** the Toxicology Unit of the BBRC (NIH NCRR Grant # 2G12RR008124-16A1), and the NSF Grant # CHE-0840525.

Abstract

Extraordinary chemical and physical properties exhibited by nanomaterials, as compared to their bulk counterparts, have made the area of nanotechnology a growing realm in the past three decades. It is the nanoscale size (from 1 to 100 nm) and the morphologies of nanomaterials that provide several properties and applications not possible for the same material in the bulk. Magnetic and optical properties, as well as surface reactivity are highly dependent on the size and morphology of the nanomaterial. Diverse nanomaterials are being widely used in molecular diagnostics as well as in medicine, electronic and optical devices. Among the most studied nanomaterials, gold nanoparticles are of special interest due to their multifunctional capabilities. For instance, spherical gold nanoparticles measuring 15-20 nm in diameter have been studied due to their insulin binding properties. Also, thiol functionalized gold nanoparticles between 5 and 30 nm are used in the detection of DNA. Thus, harnessing the shape and size of gold nanoparticles plays an important role in science and technology.

The synthesis of gold nanoparticles via the reduction of gold salts, using citrate or other reducing agents, has been widely studied. In recent years, algae, fungi, bacteria, and living plants have been used to reduce trivalent gold (Au^{3+}) to its zero oxidation state (Au^{0}) forming gold nanoparticles of different sizes and shapes. In addition, plant biomasses have also been studied for their gold-reducing power and nanoparticle formation. Although there is information about the synthesis of the gold nanoparticles by biologically based materials; to our knowledge, the study of the use of alfalfa extracts has not been reported. This innovation represents a significant improvement; that is an environmentally friendly method that does not use toxic chemicals. Also, the problem of extracting the formed gold nanoparticles from biomaterials is addressed in this research but still remains to be solved.

In this work, secondary metabolites were extracted from alfalfa biomass in liquid phase by hot water, isopropanol, and methanol, and used to reduce tetrachloroaurate ion ($AuCl_4^-$) for the synthesis of gold nanoparticles. Biosyntheses of gold nanoparticles were performed by mixing 0.75, 1.5 and 3.0 mM Au^{3+} solutions with each one of the extracts at a ratio of 3:1 respectively, and shaken at room temperature for 1h. Resulting gold colloids were characterized by UV-Vis spectrophotometry and electron microscopy techniques, showing size and morphology dependency on the reaction conditions.

Isopropanol alfalfa extracts reacted with Au^{3+} produced gold nanoparticles with a size range of 15-60 nm. The most abundant were from 40-50 nm, and the morphologies found were polygons, decahedra and icosahedra. Methanol alfalfa extracts produced monodisperse 50 nm decahedral and icosahedral gold nanoparticles. Lastly, water alfalfa extracts reacted with Au^{3+} produced triangular, truncated triangular and hexagonal nanoplates with diameters ranging from 500 nm to 4 μm and thicknesses of ~15-40 nm. The production of gold nanoplates by alfalfa extracts has never been reported before.

In order to extract the formed gold nanoparticles from the biomass, physical and chemical extractions were used. For the chemical extraction, NaCl, dilute H_2SO_4, Triton X and DI water were tested. In these cases, the best results were obtained with DI water, followed by NaCl. The extracted nanoparticles had an absorption band at about 539 nm. For the physical extractions, alfalfa biomass containing gold nanoparticles were exposed to 400 °C, 500 °C, 550 °C and 600 °C to recover the gold nanoparticles. X-ray diffractograms taken after pyrolysis of the biomass showed that the recovered nanoparticles kept their crystal structure.

Table of Contents

List of Figures

List of Illustrations

Chapter 1: Introduction

1.1 NANOMATERIALS

Nanotechnology, a term borrowed from the Greek language, involves the development, characterization, and functionalization of structures and devices with size varying between 1 and 100 nm. A significant component of nanotechnology is the production of particulate material in the size range of nanomaterials or nanoparticles. Nanomaterials (NMs) are classified as materials that have at least one dimension of 100 nm or less, while nanoparticles include materials with at least two dimensions between 1 and 100 nm[1]. Nanomaterial studies had its beginnings in the 1950's, but it wasn't until the early 1990's that nanotechnology research exponentially increased. The extraordinary chemical and physical properties exhibited by nanomaterials when compared to their bulk counterparts, have made the area of nanotechnology a growing realm in the past three decades. It is the nanoscale size (from 1 to 100 nm) and the morphologies of the nanomaterials that provide a diversity of properties and applications not possible for the same material in the bulk. Magnetic and optical properties, as well as surface reactivity are highly dependent on the size and morphology of the nanomaterial in question. Diverse nanomaterials are being widely used in molecular diagnostics as well as in medicine and electronic devices, among others [2, 3]. For instance, nano-quantum dots, which are narrowly packed semiconductor crystals embracing hundreds of thousands of atoms, are used as fluorophores in lasers, detectors, and optical devices due to their wide band gap [4]. In medicine, functionalized mesophorous silica nanoparticles (a material containing pores with diameters between 2 and 50 nm) with superparamagnetic iron oxide nanoparticles can be used for drug delivery and imaging. The superparamagnetic properties of the iron oxide nanoparticles provide the magnetic resonance and magnetic manipulation, while the mesoporous silica nanoparticles serve as a framework for multifunctional nanoparticles [5].

Monodisperse nanomaterials and nanoparticles of specific size and morphologies are fundamental in the area of nanotechnology in order to harness their properties. Many synthetic paths have been reported in the literature, both organic and inorganic, by which specific size and morphology

are achieved. Synthesis of nanoparticles is varied, yet most synthetic pathways have the commonality of using harsh chemicals for the environment. While the need to produce nanomaterials and nanoparticles is evident for the improvement of medicine, science, and technology, it is imminent that the production of such nanomaterials is done through an environmentally friendly manner. Traditional and efficient methods for the production of gold nanoparticles are widely used; however, they are expensive and in some instances, they are sources of environmental and health hazards. Developing green chemistry methodologies for the production of nanomaterials and nanoparticles will reduce the production of toxic by-products and costs in most cases [6, 7]. In the search of new methodologies, both prokaryotic and eukaryotic organisms are being studied for their applications in the production of gold nanoparticles [4, 8-12].

1.2 GOLD NANOPARTICLES

Gold nanoparticles (GNP) have been known for centuries. Since ancient times, GNPs were used for glass staining and to give the characteristic purple color to clothing used by kings. In modern science, the first known GNP production was in the 1850's. Michael Faraday was producing gold colloids by mixing gold tetrachloroauric acid ($HAuCl_4$) and black phosphorous [13]. Yet the most common synthesis is the one published by John Turkevitch in 1953, in which he was able to study the kinetics of gold nanoparticle formation by reduction of $HAuCl_4$ using citric acid ($C_6H_8O_7$) [14]. GNP synthesis by the Turkevitch method is still widely used in present times.

Gold nanoparticles have a variety of application including catalysis, medicine, and technology [15-17]. These applications are highly dependent on their catalytic, electronic, magnetic, and optical properties, as well as the surface environment of the nanoparticles. Similarly, the application of gold nanoparticles is dependent on their stability and physical properties, which are governed by their morphology and size distribution [18]. For instance, spherical gold nanoparticles of 15-20 nm are being studied for their insulin binding capacity [19]. Also thiol-functionalized gold nanoparticles with diameters between 5 and 30 nm are used for the detection of DNA sequences [20]. Harnessing the size and shape of nanoparticles plays an important role in science and technology.

In a typical gold nanoparticle synthesis such as Turkevitch, $AuCl_4^-$ is reduced to Au^0 by a reducing agent such as trisodium citrate ($C_6H_5Na_3O_7$). This method has been widely studied to understand the formation of gold nanoparticles. Illustration 4.1 shows the formation of gold nanoparticles, which starts with the addition of the trisodium citrate to a supersaturated tetrachloroaurate solution reducing Au^{3+} to Au^0. Once gold is reduced, the nucleation of Au^0 nanoparticles occurs, followed by agglomeration resulting in the formation of larger nanoparticles which is known as LaMer growth [21]. Furthermore, the addition of capping and/or stabilizing agents is needed in the typical synthesis to stop the agglomeration and achieve the desired sizes.

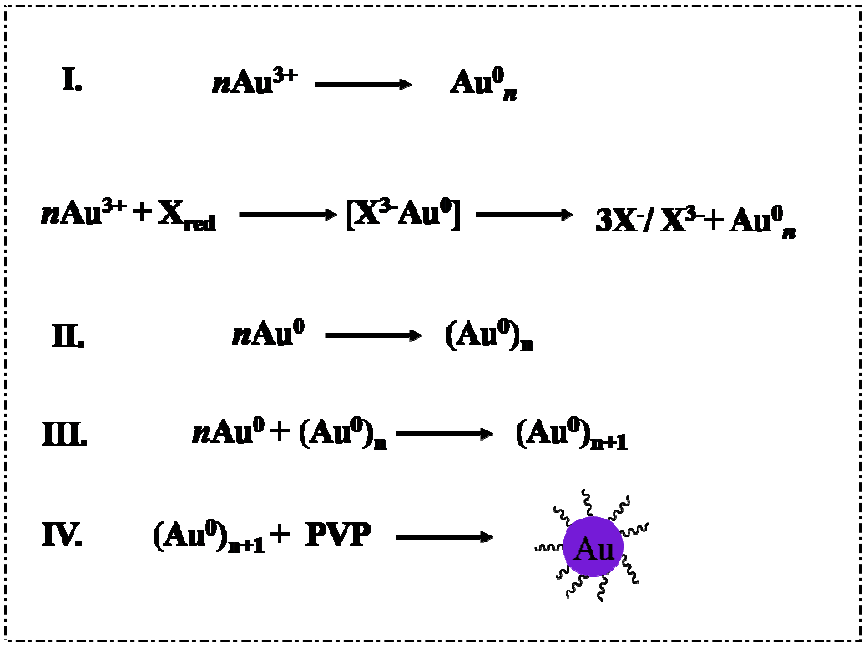

Illustration 1.1: Gold nanoparticle synthesis. I) electron transfer reduction, II) nucleation step, III) LaMer growth, IV) stabilization (adapted from Li, et al, 2008) [22].

At the beginning of the synthesis, formation of gold nanoparticles occurs when the Au^{3+} present in a high concentration gold solution reacts with a reducing agent forming an intermediate species in a fast step providing electrons to the Au^{3+}, triggering the electron transfer reaction. Once the redox reaction starts forming the gold nanoparticles, it is followed by nucleation of the nanoparticles as seen in steps I and II in Illustration 1.1. Once nanoparticles are suspended in the solution, LaMer growth takes place (step III). As long as the solution does not reach equilibrium, the growth stage continues and the

nanoparticles agglomerate into larger nanoparticles; but the addition of a capping agent or stabilizer (usually surfactants or polymer such as poly(*N*-vinyl-pirillidone) are able to control the size, as depicted by step IV in Illustration 1.1. Other reducing agents that are used for the synthesis and stabilization of gold nanoparticles include sodium borohydride and ethylene glycol. These agents are able to reduce the Au^{3+} and in the presence of the cationic surfactant poly(diallyldimethylammonium) chloride (PDDA), the formed nanoparticles are stabilized, thus inhibiting their agglomeration and growth. Some of the disadvantages of traditional synthesis are the exposure to harmful chemicals used in the process. Laboratory exposure to high amounts of ethylene glycol produces nausea, vomiting, and dizziness when inhaled. Similarly, exposure to sodium borohydride causes irritation of the mucous membranes and respiratory system through inhalation, making the use of these two very common reducing agents hazardous to health. The present approach uses alfalfa biomass as a matrix for the gold nanoparticle production as well as alfalfa biomass extracts, which, to the best of our knowledge, do not present health threats through inhalation or skin contact. Moreover, alfalfa biomass and its extracts are inexpensive in comparison to the above mentioned chemicals, and their production does not pose an environmental threat.

1.3 ALFALFA BACKGROUND

Alfalfa (*Medicago sativa* L) a member of the Leguminosae and to the tribe *Trifoliae*, is one of the most important produce in the world for its usage as forage crop for livestock, being known as the "queen of forages" among forage producers [23]. It is a perennial plant with a strong root system that elongates up to 6 m into the ground, and one of its physical characteristics is that it has yellow flowers. Alfalfa is widely distributed in temperate regions in the world and it is also able to adapt to many climates and soils. Another characteristic of alfalfa is that is has a great ability to produce high amounts of good quality seeds. Alfalfa is tolerant to temperate climates ranging from -27^{o} C to up to 50^{o} C and it is known to grow in semi-desert conditions [24]. Being a warm season perennial, alfalfa is grown in many areas of central and West Texas, including the Upper Valley in El Paso, TX and in the Mesilla Valley, NM, among other similarly warm regions.

Studies have shown that *Medicago sativa* plants contain cellulose, lignin, pectin, protein, soluble carbohydrates, starch, and lipids [25]. The amounts of these components in alfalfa vary according to species, genetics, and growth environment, among other factors. For instance, USDA researchers found that alfalfa has a high content of crude protein (127 $g \cdot kg^{-1}$ DW), lignin (158 $g \cdot kg^{-1}$ DW), and carbohydrates (563 $g \cdot kg^{-1}$ DW) [25, 26]. Other chemical compounds in alfalfa include organic acids, micro and macro minerals, and secondary metabolites such as flavonoids, and other antioxidants. Flavonoids are found in the aerial parts of different plants, providing colors present in the flowers, fruits, and leaves, as well as playing important roles in the plant development and normal growth. Moreover, flavonoids have redox properties, thus acting as Lewis acids for their hydrogen donor ability, and singlet oxygen quenchers. Moreover, it has been suggested that these compounds play an important role in the prevention of cancer by reducing the production of free radicals [27, 28].

1.4 GREEN CHEMISTRY

Scientific findings and technological advances in the twentieth and twenty first centuries have improved and elongated human life span and increased human health with the discovery of new drugs such as antibiotics, vaccines, and others. Other discoveries such as pesticides and fertilizers are widely used to improve the production of crops resulting in increased food supply for the general population. Overall, the quality of life has been improved through the discovery and use of polymers, materials and electronics not available in the past. Although these achievements are magnificent to quality of life, their developments have caused damage to the environment. Fortunately, in recent decades government agencies and communities have understood that there are significant disadvantages to the use of certain technological and scientific discoveries. The study of the negative impact of our chemical processes is the basis for several steps, including legislation and societal consciousness; which intend to remediate, reduce, and avoid further damage to the environment.

Green chemistry is defined as “carrying out chemical activities-including chemical design, manufacture, use and disposal- such that hazardous substances will not be used and generated” [6, 7]. According to the U.S. Environmental Protection Agency (EPA), green chemistry is a highly effective approach to

pollution prevention, since it consists of developing chemical processes that reduce or eliminate environmental impact [29]. Some of the principles of green chemistry include waste prevention, synthesis of less hazardous chemicals, design of safer chemicals, use of safer solvents or auxiliaries, reduction of derivatives in chemical processes, use of catalytic reagents, and the design for degradation of chemicals, such that at the end of the reaction they do not persist in the environment, among others [6, 7]. In the exploration new and safer industrial processes, the scientific community has exerted much effort in the development of chemicals, materials, and technology using the green chemistry motto. For instance, recent studies have aimed to discover new alternatives to the use of harsh solvents such in the case of the synthesis of nanomaterials. In this method, the use of ethyl acetate to blend nickel nanoparticles with poly(styrene) and its removal by vacuum, followed by the microwave assisted synthesis, proved to be a good alternative in the production of nickel-graphitic shell nanocrystals [30]. Also, nanomaterials such as Zn-Ni ferrite nanoparticles can be easily synthesized using microwave assisted combustion and urea as an alternative fuel to the most common hydrazine based fuels, which are carcinogenic. Zn-Ni ferrite nanoparticles are widely used in nanotechnology due to their magnetic properties, especially in the manufacturing of recording heads, antenna rods, loading coils, microwave devices, and as core material for power transformers in electronics and telecommunications [30]. Using solvent free procedures and the implementation of green techniques have become common place in the scientific community and reached all areas of chemistry. Green methodologies are being used for reducing harmful byproducts. Also, the use of alternative solvents in organic and inorganic chemistry is being implemented in industrial processes [31].

1.5 PREVIOUS STUDIES

The use of biological organisms to synthesize nanoparticles is a relatively new area of nanotechnology research with a high potential for growth and development. Previous studies have shown that plant biomasses as well as living plants are able to produce nanoparticles. For instance, alfalfa plants were used to form gold and silver nanoparticles intracellularly [32]. Moreover, the use of

plant extracts to synthesize gold nanoparticles has been elsewhere reported [17, 33, 34]. Aqueous extractable biochemical compounds are used in these studies and have been successful in the production of gold nanoparticles in a clean and efficient manner. Extracellular plant formation of gold nanoparticles has also been reported using geranium leaves and the endophytic fungus *Colletotrichum* sp. [33, 34]. In their work, the authors noticed that the fungus and the plants were exposed to Au^{3+} solutions where the fungus produced spherical and monodisperse nanoparticles, while the geranium leaves produced a mixture of platelets and rod like nanoparticles. Production of gold nanoparticles using alfalfa biomass of similar structure than the particles obtained by chemical methods (such as evaporation) was first reported by Gardea-Torresdey et al. (1999) [35]. In that work, alfalfa biomass was exposed to Au^{3+} solutions and gold nanoparticles were formed by the reduction of the ions. Also, that work suggested that the gold atoms were covalently bonded to the biomass, forming a stable nucleus which allowed the addition of more Au^0, thus increasing the nanoparticle size. Despite the fact that different size and morphologies of gold nanoparticles have been obtained through the exposure of Au^{3+} to alfalfa biomass, the extraction of the produced nanoparticles has been burdensome and the intended recovery had low yield [35, 36].

1.6 STATEMENT OF PURPOSE

The synthesis of gold nanoparticles using live alfalfa plants as well as hops, oat and wheat biomasses has been done in the past by our research group and others, proving to be a very cost effective and environmentally friendly method as compared to traditional synthesis. Preliminary results indicated that the nanoparticles can be removed from the biomasses using different solvents and surfactants such as sodium citrate and cetyltrimethylammonium bromide under sonication [36, 37]. Also, previous results indicated that the nanoparticles could be removed from biomass with ultrasonic radiation and surfactants such as cetyltrimethylammonium bromide (CTAB). In these studies, 1.0 mM CTAB was used followed by 3 h of sonication resulting in a small portion of nanoparticles extracted from the biomass [38]. Although the use of plants and other organisms is a promising alternative to the

synthesis of gold nanoparticles, the challenge of controlling morphology and size still remains. For instance, Armendariz et al., 2004 [10] reported that in oat biomass matrix, variations in pH resulted in the formation of gold nanoparticles of different shapes, of which the majority were 20 nm in size; however, as in other studies, the resulting particles were polydispersed. Among the most common shapes found through these methods were decahedra, icosahedra, hexagons, triangles, truncated triangles, and spheres [10, 33, 34, 37, 39-42]. Amino, carboxyl, and thiol moieties found in plant metabolites and other organisms, are believed to be responsible for the formation of nanoparticles through electron transfer and stabilization by suppressing the continuous reduction of gold. Alfalfa biomass is known to carry out the reduction of Au^{3+} to produce gold nanoparticles, as shown in previous work by electron transfer with the hydroxyl groups and covalent binding to the biomass.

Considering that the size and morphology control of gold nanoparticles is highly important for future applications, the next step required in this research was the development of an efficient method to recover the gold nanoparticles from the biomass. Furthermore, the production of gold nanoparticles more efficiently and without the use of harsh chemicals while controlling their size and morphology, was the main priority of this research. This research was performed in two separate segments. In the first segment, the production of gold nanoparticles using alfalfa biomass was be performed as previously reported. Gold nanoparticle recovery through physical and chemical extractions followed. The second segment of the research was the preparation of alfalfa extracts in liquid phase, followed by the synthesis of gold nanoparticles using those extracts as reducing agents and their further characterization.

1.7 OBJECTIVES

The general objectives of this research were:

I. To develop a plant-extract methodology for the synthesis of gold nanoparticles.

II. To develop a clean selective extraction of gold nanoparticles from alfalfa biomass.

The specific objectives were:

1. To study the formation of gold nanoparticles synthesized from the reduction of the tetrachloroaurate anion by compounds extracted from alfalfa biomass.
2. To characterize the gold nanoparticles synthesized with the extracts of alfalfa biomass using UV-Vis, Scanning Electron Microscope (SEM), Transmission Electron Microscope (TEM) and X-ray Diffraction (XRD).
3. To optimize the extraction of gold nanoparticles bound to alfalfa biomass through the use of physical and chemical extractions.
4. To characterize the gold nanoparticles extracted from alfalfa biomass using chemical and physical processes through UV-Vis spectrophotometry (UV-Vis) and XRD.

1.8 HYPOTHESIS

This research was based on the working hypothesis that certain natural compounds found in alfalfa biomass act as reducing agents and can be used in the development of a green method for the synthesis of gold nanoparticles. Furthermore, it was hypothesized that the extraction of size controlled gold nanoparticles from alfalfa biomass could be improved through physical and chemical extractions, while maintaining the original size and shape of the nanoparticles.

Chapter 2. Experimental section

All glass laboratory materials for the experiments were thoroughly washed in aqua regia (50 %) and washed three times in deionized water (DI water) to avoid metal cross contamination. The pH measurements were performed using a ROSS semi-micro pH electrode (8115BN ORION) filled with Ag/AgCl (ORION 900011). The stock solution (6 mM Au^{3+}) was stored in an amber plastic bottle to avoid photoreduction. For statistical purposes, all experiments were done in triplicate.

2.1. Methodology

Materials

Inactivated alfalfa biomass (*Medicago sativa,* cv. Malone) was used in all experiments. The biomass used was obtained from controlled agricultural fields and prepared as previously reported [43]. Briefly, alfalfa shoots were cut, thoroughly washed with water to remove debris, and oven dried at 60˚C for seven days to completely dehydrate them. Once the biomass was dehydrated, it was homogenized by grinding and sieving through a 100-mesh (149 μm) screen to achieve a uniform powder. Before each experiment, the biomass was quickly washed with 0.1 M HCl to remove soluble materials that could interfere with the binding or reduction of the Au^{3+} ions, followed by DI water wash to remove the soluble materials and neutralize the biomass. A portion of the powder was used to prepare extracts with gold-reducing capabilities and the rest was stored for later experiments. Trivalent gold in the form of potassium tetrachloroaureate salt ($KAuCl_4$) was purchased from Sigma-Aldrich (St. Louis, MO), and a 6 mM stock solution in 0.01 mM HCl was freshly prepared prior to the experiments by dissolving 0.5688 g of $KAuCl_4^-$ (Sigma-Aldrich 450235-1g) in 0.01 mM HCl (Fischer A501-212) to avoid metal precipitation, and used to make diluted solutions for the gold nanoparticles biosynthesis.

Biosynthesis of gold nanoparticles using alfalfa biomass extracts

In a 250 mL Erlenmeyer flask equipped with a condenser and a magnetic stir bar, 15 g of powder alfalfa biomass sample were suspended in 75 mL of millipore water (18 MΩ cm^{-1}), 75 mL of isopropanol, or 75 mL of methanol, and refluxed for 1 h under constant heating and stirring. The extraction was then set on a cold water bath until the extracts reached room temperature, decanted in 50 mL centrifuge tubes, and spun down at 3000 rpm for 10 min in a Marathon 8K centrifuge (Fisher Scientific, Houston, TX). The extracted supernatant was filtered through a medium pore buchner funnel with a fritted disk and used directly in the biosynthesis of gold nanoparticles. The biosynthesis was carried out in 5 mL centrifuge tubes at a 3:1 ratio of 0.75 mM, 1.5 mM, and 3 mM Au^{3+} solution:alfalfa extracts (triplicate samples), under constantly mixing in a mechanical rocker for periods of 1-24 h. Initial pH value was recorded at the beginning of the reactions, and adjusted to 2, 3, 4, 5, and 6 using different concentrations of KOH and HCl, as needed. At the end of the reaction, the nanoparticles were separated from the solvent by centrifugation, followed by a wash with ethanol then water, and followed by acetone for 10 minutes under ultrasonic motion each followed by centrifugation. A drop of sample was suspended on a carbon holey microgrid coated with a carbon film (Ted-Pella, USA) for SEM and TEM characterization. In order to corroborate the reproducibility of the technique, analyses of different samples were performed in triplicates and the reactions were repeated at least three times. For practical purposes, the alfalfa biomass extracts further in this text will be referred as: ABI for isopropanol alfalfa extracts; ABM for methanol alfalfa extracts; and as ABW for DI water alfalfa extracts.

Biosynthesis of gold nanoparticles using alfalfa biomass for the physical extractions

Portions of 9 g of alfalfa were carefully weighed and suspended in 180 mL of DI water in a 250 mL beaker to obtain a concentration of 5 mg of alfalfa per mL of solution. The alfalfa was washed in 0.1 mM HCl followed by DI water. Subsequently, the alfalfa was centrifuged in order to remove excess material that could interfere with the Au^{3+} binding to the alfalfa biomass. The alfalfa pellet was resuspended in 3.0 mM Au^{3+} solution and mixed in a magnetic stirrer while the pH was being adjusted to 4 using hydrochloric acid and potassium hydroxide solutions as needed (0.01-1.0 mM). The

suspensions were then placed on a heating mantle and stirred continuously under heat until the reduction of Au^{3+} took place, which was evident by the appearance of purple color. After 15 minutes, the purple slurry (Alfalfa/AuNP matrix) was removed from the heat and cooled at room temperature, followed by centrifugation at 3000 rpm (Marathon 8K, Fischer Scientific, Pittsburg, PA) and the supernatant was separated from the pellet. The pellet containing the Au nanoparticles was then washed twice with DI water and centrifuged at 3000 rpm for 10 min. The Au nanoparticle/alfalfa biomass (Alfalfa/AuNP) pellet was then dried in an oven at 60^{o} C for 1 h, and used for the chemical and physical extractions. A blank experiment was performed by placing 100 mL of 3 mM Au^{3+} under the same conditions as the alfalfa/Au experiment above.

Chemical extractions of Au nanoparticles from alfalfa/AuNP matrix

Extraction of gold nanoparticles from the alfalfa/AuNP matrix was performed. For each extraction, 100 mg of alfalfa/AuNP was weighed and suspended in 40 mL of solvent to extract the nanoparticles from the matrix. The solvents chosen in this experiment were DI water, NaCl (1M), Triton X (10% v/v), and H_2SO_4 (1% v/v). The alfalfa/AuNP in the respective solvent was sonicated for 2 min at 50% power followed by centrifugation at 3000 rpm and phase separation, based on previous work done by Armendariz et al. 2004 [40] and analyzed using a UV-Vis spectrophotometer. Sample blanks for the samples were chosen according to the solvent used in each experiment. The alfalfa/AuNP was dried at 80^{o} C and homogenized using a mortar and pestle for further analysis.

Physical extraction from alfalfa/AuNP matrix

In order to extract the gold nanoparticles form the alfalfa/AuNP matrix, one gram of samples were ashed by exposure to 400, 450, 500, 550, and 600°C for 24 h in a muffled furnace (Type K T/K 0.5Ω, model J-100, Satellite Manufacturing Company Inc, Los Angeles, CA) for the pyrolysis of organic matter in the alfalfa/AuNP matrix. The ashing of the samples allowed recovering the gold nanoparticles which were then analyzed by X-ray fluorescence and X-ray diffraction.

2.2 Characterization

Spectrophotometric, X-ray fluorescence and X-ray diffraction characterization

The supernatant of the first extraction was analyzed by UV-Vis (Cary 50, 2002 VARIAN Inc, Australia Pty Ltd) to determine the extraction performance. Quartz cells were used for the UV-Vis analysis. A single scan from 800 to 200 nm at a scan rate of 300 nm min^{-1} was done in all samples with a zero/baseline correction. The homogenized alfalfa/AuNP matrix was analyzed by X-ray fluorescence in a High Performance Energy Dispersive X-ray Fluorescence instrument (XRF-XDAL), Fischerscope (Helmut Fischer, Sindelfingen, Germany) with a measuring distance from 20-80 mm for qualitative analysis showing Au as the only metal present in the sample. The same sample was then analyzed by X-ray diffraction using a copper anode target and the Cu K_α (1.5406 Å) with a D8 DISCOVER X-ray diffractometer (Bruker). The samples were scanned from 20 to 90 degrees in 2θ, with a scan speed of 5° min^{-1}.

Microscopic characterization

The produced gold nanoparticles were characterized by atomic force microscope (AFM), scanning electron microscope (SEM) and transmission electron microscope (TEM). Tapping mode AFM imaging was carried out with a Nanoscope V AFM (multimode, VEECO instruments) using phosphorus doped silicon probes. The sample for imaging was prepared by dispersing the prepared Au nanoparticles in ethanol/water and adding a drop of the solution to a pre-cleaned silicon substrate. The nanoparticles were then allowed to dry slowly. The Si substrate containing the sample was then used to perform AFM imaging and measurements. The SEM characterization was performed via a FEG Hitachi S-5500 ultra high resolution scanning electron microscope (0.4 nm at 30kV) with BF/DF Duo-STEM detector and a FEG Hitachi S-4800 high resolution scanning electron microscope (1.0 nm at 30 kV) with a BSE and SE detector. The TEM analyses were performed in a JEOL JEM-2010F equipped with a field

emission gun and operated at 200 kV with a 0.1 nm lattice resolution; and a Hitachi H-9500 300 kV transmission electron microscope (0.1 nm at 300kV). High resolution transmission electron microscopy (HRTEM), selected area electron diffraction (SAED), and weak beam dark field (WBDF) analyses were performed using a Philips Tecnai G^2 TEM equipped with Schottky-type field emission gun, ultra-high resolution pole piece (Cs=0.5 mm), and a scanning transmission electron microscope (STEM) unit with a high angle annular dark field (HAADF) detector operating at 200 kV. A sample drop was suspended on a copper microgrid coated with a carbon film (Ted-Pella, USA) and left to air dry for SEM and TEM analysis.

Chapter 3: Instrumentation

3.1 FUNDAMENTALS OF SPECTROPHOTOMETRY

Electromagnetic radiation is energy that propagates at the speed of light by an electromagnetic field. The electromagnetic (EM) spectrum is defined as the ordered arrangement of electromagnetic radiation according to wavelength, wave number, or frequency [44]. The EM spectrum includes gamma rays, X-rays, ultraviolet (UV), visible (Vis), infra-red, micro and radio waves with wavelengths from less than a picometer to more than a meter. The UV and Visible regions (UV-Vis) fall in the range of 200-380 nm, and 380-780 nm, respectively. This is the region that is used in spectrophotometry to obtain information about interactions of molecules and ions [45].

When a liquid, solid or gas sample is exposed to electromagnetic radiation, a number of processes occur including absorption, diffraction, reflection, refraction, transmission or scattering of the radiation by the molecules or atoms in the sample. These processes are harnessed in different ways to provide information about the sample such as concentration, composition, crystal structure, and intermolecular interactions, among others. The magnetic component of electromagnetic radiation is responsible for the absorption of radio frequency waves by atoms and molecules; this is the basis for nuclear magnetic resonance. On the other hand, the electric component of the electromagnetic radiation is responsible for the absorption of radiation by the samples. The interaction between a sample and an incident radiation, and the processes of absorption and emission are illustrated below (Illustration 2.1). Before the incident radiation hits the sample, the atoms are found in the ground state (most stable configuration). After being bombarded with the radiation of the right magnitude, the energy is absorbed by the atom and the electrons in the outer shells are promoted to higher energy levels (excited state) [45].

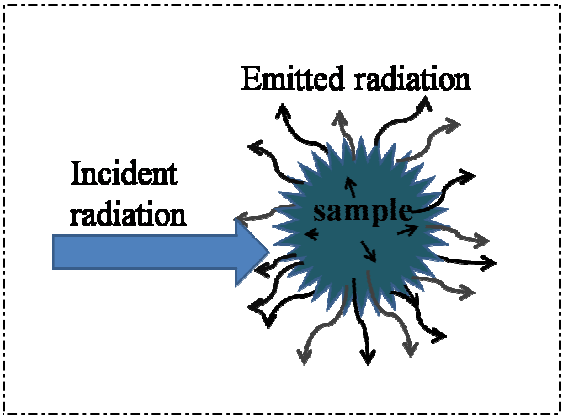

Illustration 2.1: Emission process, as a sample is excited absorbs and emits radiation [45].

As mentioned above, in absorption spectrophotometry, a sample is exposed to radiation promoting the atoms to a higher energy; and as the atoms decay to a ground state, the emitted wavelengths are measured. Since the wavelengths emitted by the molecules or atoms are proportional to the electronic transitions occurred, it is possible to determine exactly the identity of such elements in the sample [45]. For example, energy transitions occurring in the d electrons in transition metals are responsible for the color; such is the case of chromium, copper, and cobalt which are used as examples for colorimetric analyses. Illustration 2.2 shows the process occurring as the sample is bombarded with radiation (2.2a).

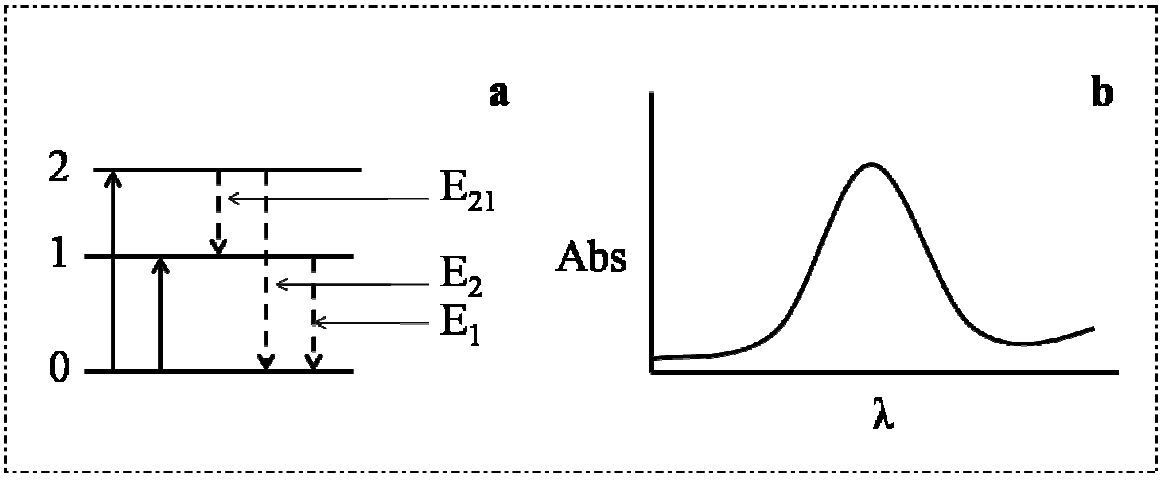

Illustration 2.2 a) Energy transitions from ground state to excited state, the dotted lines represent radiation emitted as the species go back to the ground state, b) Characteristic absorption spectrum from a spectrophotometer analysis [45].

In order to understand the relationship between energy transitions and absorption processes, it is important to consider quantum theory; which states that atoms, molecules, and ions have a limited amount of discrete energy levels, and in order for absorption to occur, the energy of the exiting photon must be the same as the difference in the energy of the ground and excited states of the sample. Illustration 2.2a shows the resulting transitions in the energy levels once the species in a sample are exposed to radiation and excited to higher energy levels. The characteristic absorption spectra for absorption spectrophotometric analysis can be seen in illustration 2.2b.

3.1.1 UV-Vis spectrophotometry

A UV-Vis spectrophotometer is able to detect radiation in the range of 200-780 nm and provide information to identify species such as molecules and ions in a sample. Atomic or molecular species (M) in a sample absorb UV-Vis radiation by a two-step process in which the species are first promoted to a higher energy state that is generated by the excitation of bonding electrons known as electronic excitation ($M + h\nu \rightarrow M^*$). This is followed by the relaxation of the species which generates radiation, sometimes as heat ($M^* \rightarrow M + h\nu$/heat). The electrons involved in electronic transitions include the π and σ (bonding), and *n* (non-bonding) electrons, *d* and *f* electrons, and charge transfer electrons. Among the species containing π, σ and *n* electrons, are the organic molecules and ions such as benzene and naphthalene in the UV range ($\sigma \rightarrow \sigma^*$ transitions). Absorption of longer wavelength radiation is restricted to functional groups that contain valence electrons with low excitation energies known as chromophores ($\pi \rightarrow \pi^*$ transitions), and some inorganic ions such as carbonate ($n \rightarrow \pi^*$ transitions). Absorption spectra of transition metals, actinides and lantanides are due to *d* and *f* electron transitions among the different orbitals' energy levels [45].

In spectrophotometric analysis, the intensity being absorbed is measured before and after the sample is exposed to radiation because once it passes through the sample, very selective frequencies are removed by the absorption process. Since this energy differences are specific for each species, it is possible to identify specific compounds or elements, based on these frequencies, and measure their concentration. A relationship between the absorbed radiation and the concentration of species can be

drawn from Beer's Law, where A is the absorbance, b is the pathlenght, c is the concentration of the species in question, and ε is the molar absorptivity coefficient. In this equation, the absorbance is proportional to the log of the ratio between initial and final intensity of radiation.

$$A = \varepsilon bc, where\ A = \log \frac{Po}{P} \qquad \text{Eq. 1}$$

There are five components in a typical spectrophotometer: 1) the radiation source, usually a tungsten lamp, that is able to cover the required wavelength range, in this case it is 2000-8000 Å (200-800 nm); 2) the monochromator, which is a device that selects narrow wavelengths to be used in specific measurements; 3) the sample holder, which is the compartment where the sample is kept during analysis; 4) the detector, which measures the intensity of the radiation beam transmitted through the sample in the cells; and 5) the output display, which is the computer that converts the signals to data [45]. The general arrangement of a typical spectrophotometer and its components is shown in illustration 3.1.

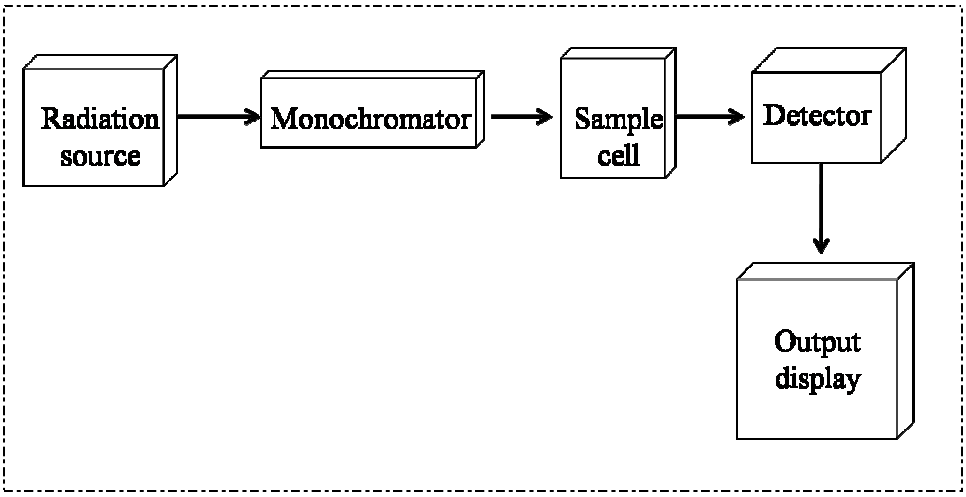

Illustration 3.1: Basic arrangement of the UV-Vis spectrophotometer components [45].

3.2 FUNDAMENTALS OF X-RAY DIFFRACTION AND X-RAY FLUORESCENCE

X-rays are short wavelength, high energy electromagnetic radiation of energies between 1 Å to 100 Å (0.01 nm- 10 nm), but in X-ray diffraction, only a portion of the spectrum having wavelengths of 0.3 Å to 2.5 Å are used [46]. If a sample is bombarded with X-rays, the diffraction process occurs and this technique is called X-ray diffraction. X-rays that are produced when the electrons in the shells of atoms are bombarded by a beam of high energy electrons are diffracted by the atoms in the sample. The high energy electrons are produced by an external source such as an X-ray tube or an electron gun. The X-ray tube consists of two metal electrodes (anode and cathode) confined in a vacuum chamber. The radiation is produced through heating a tungsten filament (the cathode) and the emitted electrons are accelerated toward the anode. Once the electrons collide with the anode, most of the energy is lost as heat, but some of the electron energy is manifested as X-rays [46, 47]. As mentioned earlier, the energy loss of the electrons as they go back to the ground state is compensated and expressed by different processes, one of which is continuum radiation, also known as white radiation or Bremsstrahlung. Illustration 3.2 shows the characteristic X-ray spectra from a copper target.

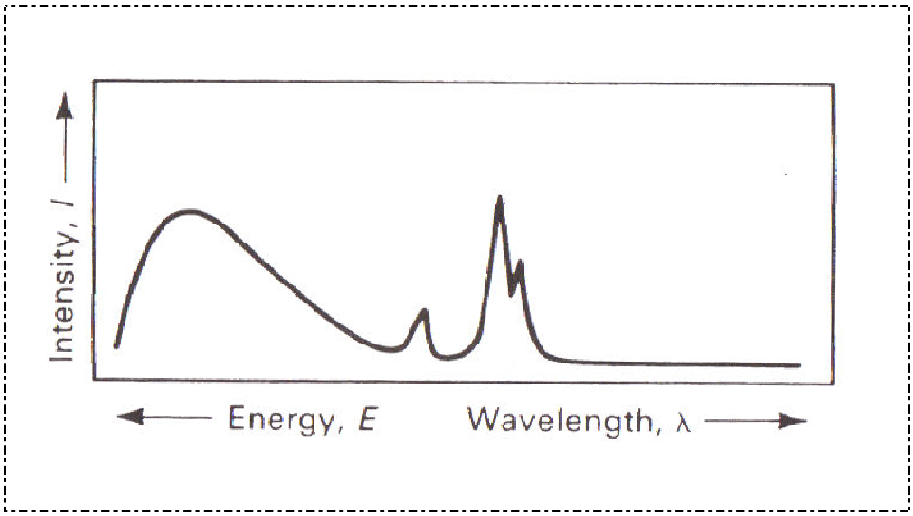

Illustration 3.2: Characteristic x-ray spectra (after Smith 2008) [46].

As seen in the illustration, the wide band part of the spectra at lower energy (to the left) is the Bremsstrahlung radiation, and only a few sharper peaks are the high energy X-rays superimposed in the Bremsstrahlung radiation spectra. The target typically used in X-ray diffraction is copper since its K_α

(1.5406 Å) characteristic radiation is useful for diffraction analysis for gold and various metals, as well as other crystalline materials. All X-ray diffraction analyses in this research were done using the Cu K_α radiation.

X-ray diffraction is the preferred technique for phase characterization of materials in powder form or in aggregates of finely divided materials, because it can differentiate between phases of the same material having the same chemical composition but different crystal structure [46]. Diffraction occurs when a high energy electron beam hits a sample surface and the electrons in the beam collide with the electrons in the atoms, modifying the behavior of the waves as they interact with the atoms. When the incident beam interacts with the atoms in the molecule, the electric vector of the beam gets in contact with the electrons in the sample to produce diffraction. The waves are diffracted by the atoms in the forward direction and since the incident beams are parallel, they make an angle with the sample surface (θ). As a result, the diffracted beams 1' and 2' are in phase (as seen in illustration 3.3) and diffraction occurs.

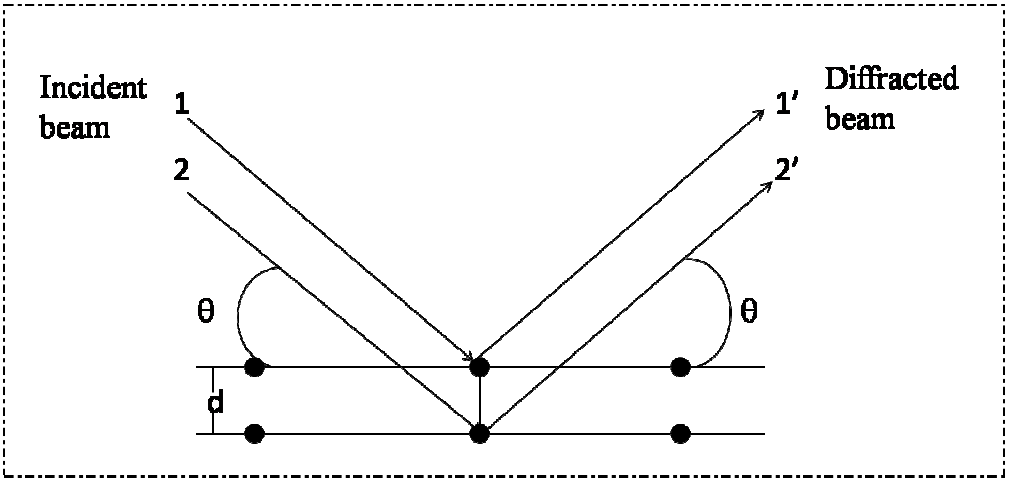

Illustration 3.3: X-ray diffraction process, 1 and 2 are the incident beams, 1' and 2' are the diffracted X-rays in phase, d is the spacing between the path lengths of the beams [44].

The diffraction model can also be understood by analyzing Bragg's law, which was formulated by W. L Bragg in 1913, and determines the interference pattern of the X-rays diffracted by the atoms, ions or molecules in a sample by assuming that the each plane of atoms scatters the incident radiation wave according to the spacing of the atomic planes. Also, the diffraction of the wavelengths must be in

phase, producing constructive interference at restricted angles (known as Bragg angles) so that the conditions are satisfied and the law can be applied. Equation 2 shows the customary form of Bragg's Law [47].

$$n\lambda = 2dsin\theta \qquad \text{Eq 2.}$$

Where n is an integer, and *d* is the interplanar distance of the crystal, λ is the CuK_α wavelength (1.5418 Å). As mentioned earlier, X-rays are diffracted only if the Bragg condition is met, which occurs when the spacing between layers of atoms on the surface of the sample are close to the same wavelength of the radiation, and when the scattering centers are regularly distributed in space so the X-rays are reflected form the sample [45]. The diffraction of the X-rays in this case, is very useful to determine the crystal structure and phase of a material. Once the sample is hit by the radiation, diffraction of characteristic wavelengths become apparent in the emitted spectrum, and can be used through the use of equations to obtain physical and chemical information. The information obtained from the peaks includes the d-spacing, which in combination with Bragg's Law, miller indices, and lattice geometry equations, provide the solution for the crystal structure and phase of the sample being analyzed. Also, average particle size can be determined from X-ray diffraction by using Scherrer's equation, which was derived by P. Scherrer in the early 1900's, and it takes into consideration the fact that smaller particles produce broader diffraction peaks. Equation 3 is the derived form of the Scherrer's equation.

$$d = \frac{k\lambda}{BCos\frac{2\theta}{2}} \qquad \text{Eq. 3}$$

Where *d* is the particle size measured in a direction perpendicular to the specimen surface, B is the full width half maximum of the diffraction peak in radians (FWHM), λ is the Cu K_α radiation, θ is the Bragg angle, and k is a constant with value of 0.94 [47].

X-ray fluorescence (XRF) is a process in which an incident beam of X-ray radiation is applied to a sample and the resulting radiation (fluorescence) is characteristic of the element present [48]. The generation of X-ray fluorescence can be explained by the photoelectric effect which states that when a beam from an X-ray tube interacts with the sample; an electron is excited and gets promoted to a higher orbital leaving an empty space. The empty orbital is then filled by electrons from outer shells, and fluorescence occurs, as depicted in illustration 3.4. The electron is ejected and the empty space is filled by an electron from an outer shell, emitting an x-ray photon (fluorescence) or an auger electron because the binding energy is decreased (as compared to the binding energy of the higher energy electrons). When this process takes place, the X-ray fluorescence energy is lower than the ionization energy, and the fluorescence radiation characteristic of the species (illustrated as secondary radiation), is generated. Since the fluorescence is proportional to the energy of the electrons being ejected, this makes possible the determination of the sample composition [49].

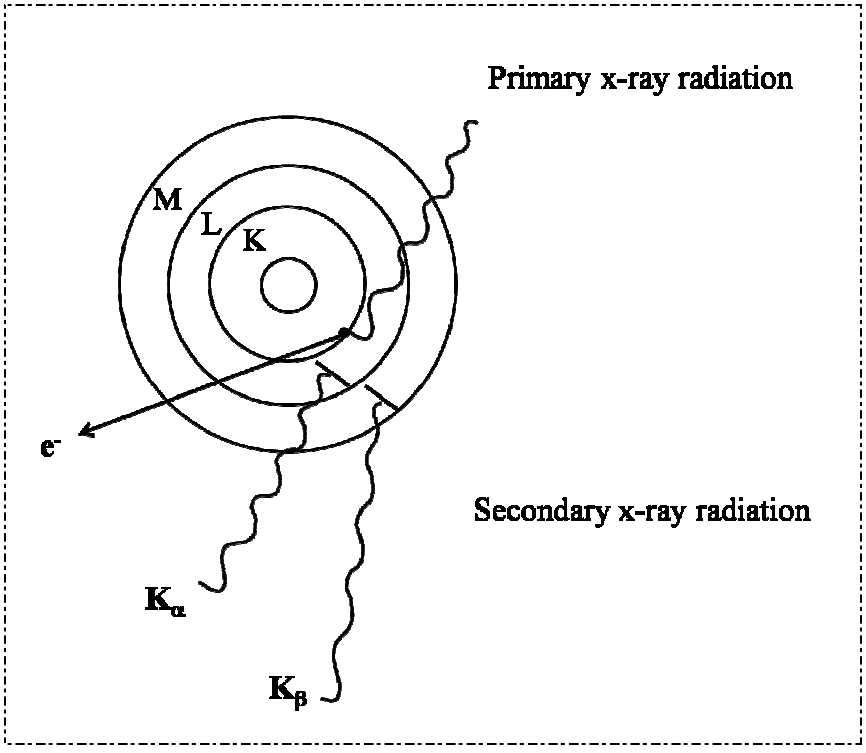

Illustration 3.4: X-ray fluorescence process, generation of the X-ray fluorescence radiation (adapted from ASM handbook) [44].

X-ray fluorescence, is a good characterization technique mainly used for bulk samples because it allows the determination of elemental composition with little or no sample preparation required, making it a non destructive analytical technique. Identification of elements in a sample occurs through their characteristic wavelengths, and their concentration can be obtained by the intensity of the peaks using a calibration curve of known concentrations of the elements in question. Other advantages of XRF include measurements of a wide range of elements (from aluminum to uranium) in various solid samples at room temperature and normal environments.

3.3 FUNDAMENTALS OF MICROSCOPY

3.3.1 Scanning electron microscopy

Scanning electron microscopy (SEM) is a technique for material characterization widely used due to its high resolution. The images provided by SEM are very similar to those seen by the human eye but at a high magnification and a resolution of 1 Å. The source of radiation is a probe lens that ejects accelerated electrons of a potential between 5 kV and 30 kV. When the highly accelerated electrons interact with the sample, the scattered events occurring depend on the thickness of the sample and the accelerating voltage of the electron beam. For instance, if the sample is very thin, some electrons pass through the sample (transmitted electrons) and other electrons are scattered. Electron scattering is classified in two groups: elastic and inelastic collisions. Elastically scattered electrons change their direction but conserve the velocity or energy while backscattered electrons (BSE) are produced by this kind of collision. Inelastically scattered electrons, on the other hand, are characterized by the loss of energy. Inelastic scattering occurs through various processes including production of phoneus (heat), characteristic X-rays, continuum X-rays, auger electrons, and secondary electrons (SE) [50].

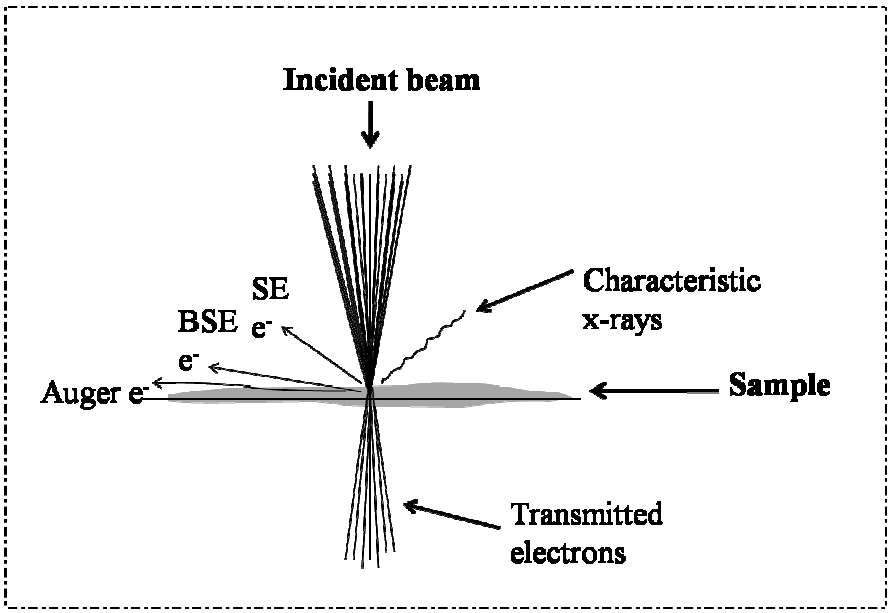

Illustration 3.5: Scattering processes upon electron beam and sample interaction.

Secondary electrons are bound to the outer shell of the sample atoms and as they receive enough energy from the beam, they get ejected from the atom and propagate through the sample until some of them are able to escape and produce the image. The SEM uses both backscattered and secondary electrons, and X-rays as the main signals for image formation. High resolutions can be between 20-50 nm and the lowest resolution is in the micro-meter scale. Magnification can be in the 10X to 100,000X range, giving the technique its broad applications in material characterization and nanotechnology [50]. Image formation in the SEM is a complex process; first, the high energy electrons are focused on a fine beam which rasters an entire surface of the sample. Then the image is obtained by scanning the probe over the sample and the signal is amplified and processed. A probe lens is used in SEM to determine the resolution and to focus the beam onto the sample. The probe lens is located above the sample, and the beam has sufficient energy to eject secondary and backscattered electrons from the sample (refer to Illustration 3.5). Secondary electrons are a good and common signal used in SEM because they are emitted from a space close to the beam and are easily detected, forming a high resolution image. Backscattered electrons also escape from the sample and are sometimes used as a signal depending on the microscope. Backscattered electrons or secondary electrons are collected in a specific detector, and the signals collected are amplified and displayed in a cathode ray tube.

3.3.2 Transmission Electron Microscopy (TEM)

In transmission electron microscopy (TEM), electrons are emitted from an electron gun. These transmitted electrons are accelerated toward the sample through a high vacuum column and passed through a set of lenses that are incident to the sample. Once the incident beam passes through the sample, which has to be very thin, and the transmitted electrons (see illustration 3.6) are accelerated through the lenses, they form an image of the sample in a fluorescent screen and then are sent to a camera where the images can be recorded in a digital format or in film as previous models of TEM. Although the source of radiation in both SEM and TEM are accelerated electrons, the working principles are different as seen in the components and microscope setup in illustration 3.6.

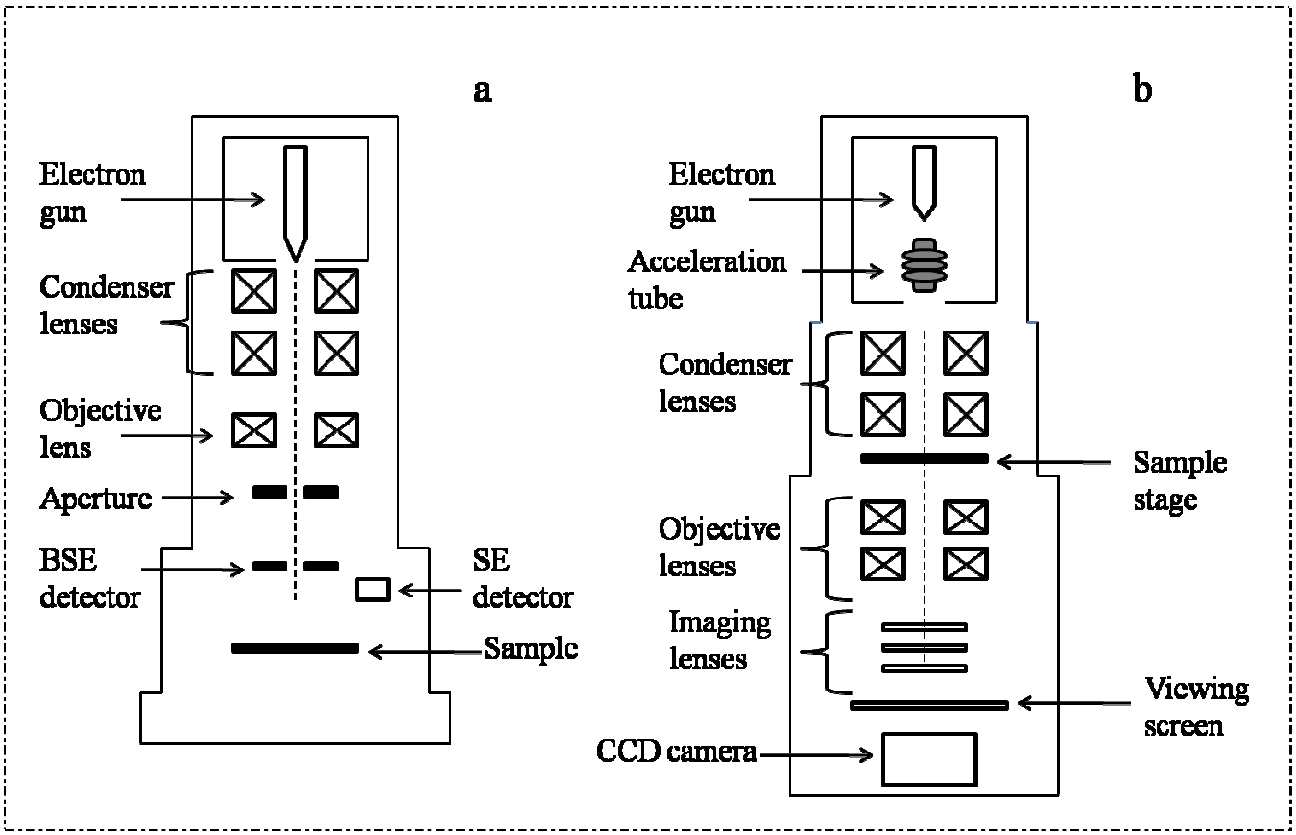

Illustration 3.6: Basic components of: a) scanning electron microscope (SEM) and b) transmission electron microscope (TEM)

In a TEM, the electron gun is also located above the sample, at the top of the column. Electron guns used in transmission electron microscopy include the thermionic gun and the field emission gun (FEG). The difference among both kinds is that the thermionic gun uses a tungsten filament or a

lanthanum hexaborate crystal filament, while the field emission gun does not use a filament. Instead, FEG generates the electrons by field emission, which occurs when a strong electrical field is applied to the surface of a metal, and the electrons are emitted from the surface passing through a potential in a "tunneling" effect [51]. FEG is more widely used in modern microscopes because it produces brighter and more coherent electrons, providing a better spatial resolution that the thermionic gun. The illuminator lenses' function is to converge the beam on the sample, and that of the deflector's is to tilt, shift or scan the beam while controlling the beam onto the sample. Once the converged beam passes through a small area of the sample, the transmitted electrons go to the objective lens where the image is formed, followed by signal processing and digital display of the image [51].

3.3.3 Atomic Force Microscopy

Atomic force microscopy (AFM) is used to study surface characteristics of samples. The AFM works through atom-tip interaction at the nanometer range by rastering the tip along a sample with a probe very close to the sample surface. This interaction allows the measurement of attractive or repulsive forces between the probe and the sample at a constant force mode (height), thus creating a three-dimensional image of the sample surface with resolution at the atomic level [52].

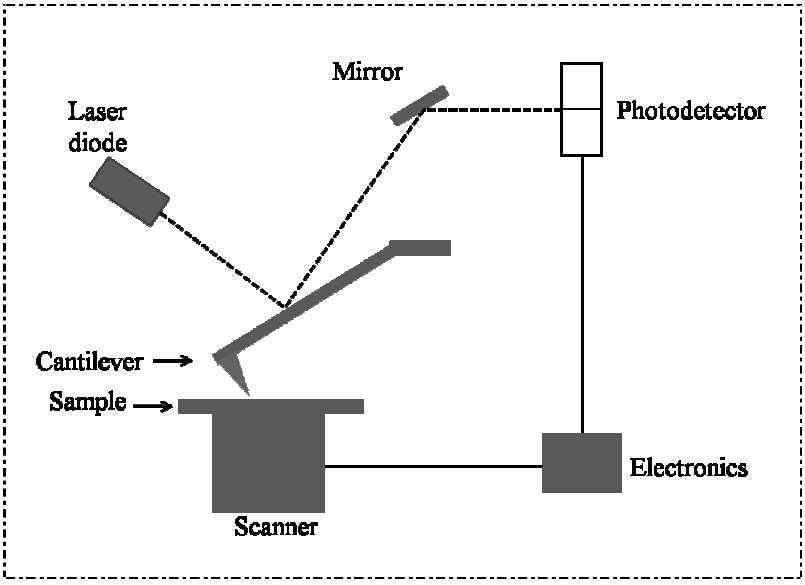

Illustration 3.7: Block diagram of the basic components of an atomic force microscope [52].

The AFM instrumental arrangement is shown in Illustration 3.7. The main components of the AFM are the tip, cantilever, laser diode, mirror, photodetector, scanner and electronics. The image is formed by recording the force interactions as the sample is scanned on the surface by the cantilever. The scanner, which is made of a piezoelectric tube, is used to move the tip over the sample, or vice versa to form the image. In order to obtain the image, the sample is positioned on the scanner and the diode laser light is directed to the end of the cantilever, which is then reflected by the mirror to the photodiode while the sample is being scanned. The attractive or repulsive forces (which include van der Waals, electrostatic, hydrophobic, hydrophilic, and capillary) between the sample and the tip bend the cantilever directing the deflected laser beam to the mirror and then to the position-sensitive photodetector, which is composed of two side-by side photodiodes that provide the topographic information of the sample surface [52, 53]. AFM provides topographical information on samples with a vertical resolution at the micrometer to the nanometer range not seen in other microscopes. Other advantages of this technique include the ability to image samples in gaseous and liquid media, as well as to provide quantitative height information [53]. This surface scanning technique also enables the gathering of spatial resolved information on the surface of a solid.

Chapter 4: Results and Discussion

In this work, alfalfa biomass extracts were used as reducing agents for the formation of gold nanoparticles. Plants including alfalfa produce many secondary metabolites, which are easily extracted using green solvents such as water and alcohols. Some of these secondary metabolites include terpenoids and polyphenols such as flavonoids, flavonols, flavanones, anthocyanins and isoflavones [54]. Alfalfa extracts contain such metabolites and other macromolecules including protein, which has amino and carboxyl moieties. It also contains other carbohydrates and organic acids as reported in the literature [23, 25]. Reports on secondary metabolite extractions using methanol as the extracting solvent, have shown that apigenin and luteolin glycosides are among the most common flavonoids in alfalfa extracts. Flavonoids are organic molecules know for their functional groups such as hydroxyl, and carboxyl moieties [25] that act as reducing entities and facilitate the formation of gold nanoparticles through electron transfer mechanisms. Hydroxyl, carboxyl, thiol, and amino moieties are known for their reducing power, and when mixed with a strong oxidizing agent, such as Au^{3+}, redox reactions are very favorable.

Reduction as well as stabilization of the gold nanoparticles biosynthesized by the alfalfa biomass extracts occurs in the presence of reducing species via electron transfer reduction in a similar fashion as the traditional synthesis. The most abundant functional groups in these compounds are carboxylic acids, carbonyls and phenols which have a great reducing potential for metal ions such as Au^{3+}. The reduction of the tetrachloroaurate ion by a phenol group in one of the flavonoids present in the alfalfa extracts can happen via electron transfer and the stabilization of the nanoparticles by other compounds present in the extracts such as amino and thiol moieties, from proteins within the same plant extract mixture. It is known that pH of the reducing environment and the reducing agents affect the size and morphology of the nanoparticles [37]. For this reason, pH and concentration profile experiments were performed to study the formation of gold nanoparticles under different conditions.

4.1 BIOSYNTHESIS OF GOLD NANOPARTICLES USING ALFALFA BIOMASS EXTRACTS

4.1.1 pH profile

Three different solvents were used in the preparation of the alfalfa biomass extracts. These solvents were chosen due to their wide availability and minimal damage to health and the environment. Alfalfa biomass extracts prepared in isopropanol (ABI), methanol (ABM) and water (ABW) were reacted with tetrachloroaurate ions in solution at varying pH resulting in nanoparticles of different size and morphologies. The reduction of Au^{3+} ions by exposure to alfalfa biomass extracts prepared in different solvents was monitored by UV-Vis spectrophotometry. Figure 4.1 depicts the spectra of the formation of gold nanoparticles at different pH. Au^{3+} reduction in alfalfa biomass isopropanol extracts and formation of gold nanoparticles happened in the whole pH range tested (Figure 4.1a) with the exception of alfalfa extracts produced in methanol which only produced the nanoparticles at pH 2 (Figure 4.1b).

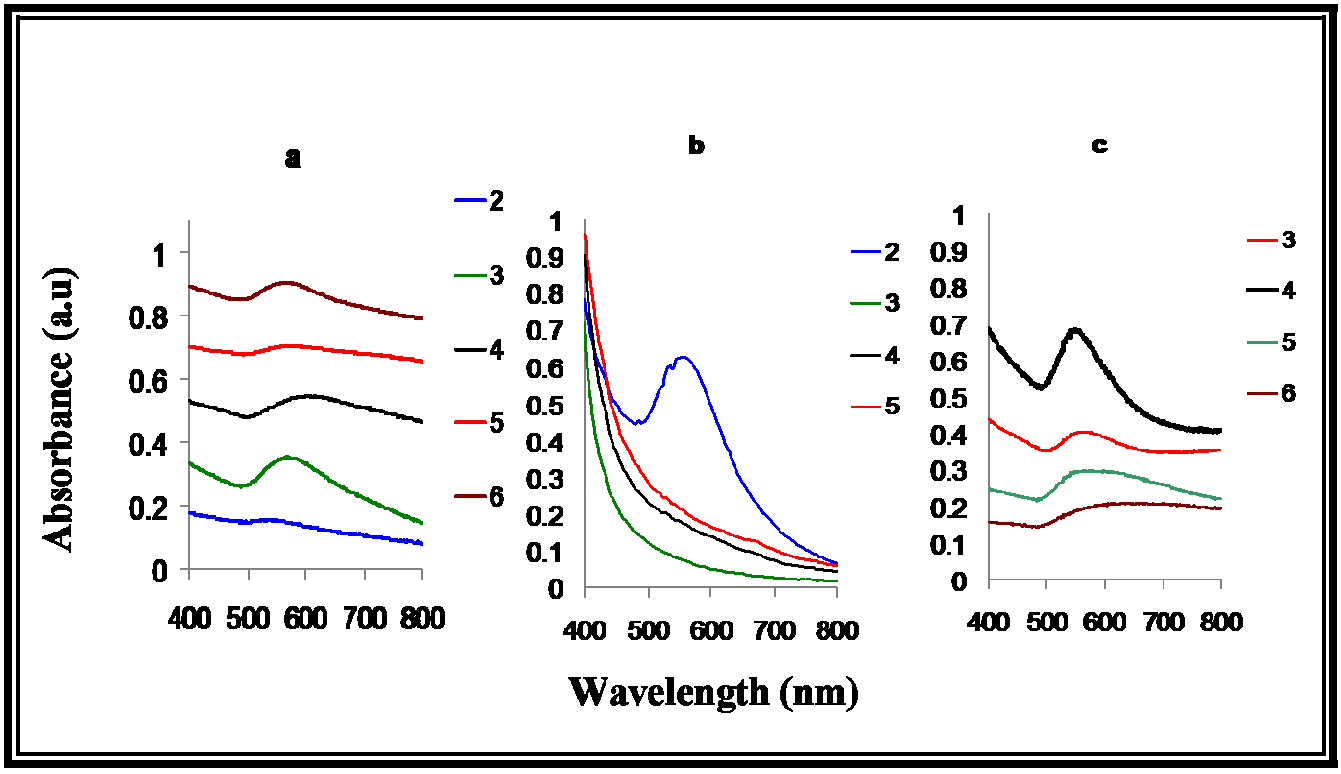

Figure 4.1: pH profile for the reduction of tetrachloroaurate ion and production of gold nanoparticles in alfalfa extracts prepared in different solvents: a) isopropanol alfalfa biomass extracts, b) methanol alfalfa biomass extracts, and c) water alfalfa biomass extracts .

As seen in Figure 4.1a, gold nanoparticles were formed at pH 2, 3, 4 and 5, but the sharper and more defined absorption band maxima was at 565 nm and solution pH of 3. On the other hand, the behavior of nanoparticles in Au^{3+} solution exposed to alfalfa biomass methanol extracts only formed at pH 2 with an absorption band maxima at 560 nm (Figure 4.1b). Lastly, the reduction of Au^{3+} in alfalfa biomass extracts in water did not show great variations in ph 3 and 4; however, at pH 5 there is no nanoparticle formation and at pH 6 the absorbance band is wide, showing dispersion in the size of the nanoparticles (Figure 4.1c). From these results, it was concluded that the reduction of the Au^{3+} ions and the formation of gold nanoparticles are dependent on the electron transfer between the gold ions and the compounds in the three different extracts. As mentioned earlier, the chemical composition of the alfalfa extracts include flavones and flavonoids with plenty of reducing hydroxyl species providing the necessary energy for the electron transfer to occur in the reduction of $Au^{3+.}$ Based on these results, the preferred pH for the production of gold nanoparticles were 2, 3 and 3.5 for methanol, isopropanol, and water, respectively. At a low pH, the hydroxyl moieties of the compounds present in the extracts can be oxidized to their respective carbonyl compounds, which is proven in the results obtained.

4.1.2 Concentration profile

High concentrations of Au^{3+} ions are required for the reduction and nucleation of the nanoparticles to take place during nanoparticle synthesis. Nucleation must occur in a short period of time, and one way of monitoring the nucleation rate in this research was to vary the concentrations of gold in the reaction mixture [1]. The concentration profile for nanoparticle biosynthesis in isopropanol alfalfa biomass extracts is shown in Figure 4.2a. In a stopped-flow kinetics experiment, a sample was taken immediately after the reaction was started at different time points and analyzed at 565 nm for a total time of 240 min. The results indicate, as seen in the figure, that the reduction and nucleation start as soon as the reducing agents are added to the Au^{3+} solution in all concentrations. Our results are in accordance with the literature stating that reduction of Au^{3+} in the presence of reducing agents occurs as rapidly as 20 seconds [55]. The kinetic data shows that at the highest concentration of Au^{3+} (3.0 mM), a rapid increase in absorbance occurs in the first 30 minutes at which reduction and nucleation occur.

Aggregation and growth occur between 30 and 50 minutes, and a sudden decrease in absorbance follows. Since the concentration of extract is much smaller than the concentration of Au^{3+} ions in the solution, the maximum agglomeration and growth are achieved in one hour. In comparison, gold nanoparticle formation at the lowest Au^{3+} concentration used in the experiments, 0.75 mM, was not very favorable at the beginning of the reaction thus agglomeration and growth were very slow. As seen in the figure, the slope of the reaction was smaller in the first 60 minutes, followed by a higher increase as opposed to the faster reaction rates observed in the higher concentrations of Au^{3+}. This implies that the reduction and nucleation steps are slower and less efficient than the 3.0 mM concentration of gold ions. The gold nanoparticles produced in the best conditions were further characterized for size and shape; the results are discussed further in the next section.

Formation of gold nanoparticles in ABM is shown in Figure 4.2b. As seen in the figure, reduction of Au^{3+} occurs immediately after addition of the reducing agents (extract), showing an absorbance of 0.7, 0.35 and 0.1 a. u for Au^{3+} concentrations of 0.75, 1.5, and 3.0 mM, respectively. The nucleation and growth of the nanoparticles exhibit a similar trend in the two lower concentrations. The reaction mixture with 3 mM Au^{3+} shows a different result. In this reaction, the reduction step occurs at a lower rate and the agglomeration and growth are reached after 20 minutes, but the absorbance is constant all through the end of the experiment. This result allows us to assume that the nanoparticles being formed do not further agglomerate and grow as it occurred with the isopropanol extracts after 20 minutes. It is also possible that the flavonoids, organic acids, aminoacids and other molecules found in the extracts can act both as reducing and stabilizing agents during nanoparticle formation in the reaction. This can be explained by the high oxidizing potential of Au^{3+} and its ability to oxidize the hydroxyl moieties as well as primary and secondary carbons found in the molecules present in the sample. The formation and stabilization of the gold nanoparticles is also observed by comparing the color of the nanoparticles in solution (Figure 4.2 and b insets). Further characterization showed that this assumption is correct as discussed in further sections. Stopped flow kinetics of gold nanoparticle formation in ABW results are shown in Figure 4.2c.

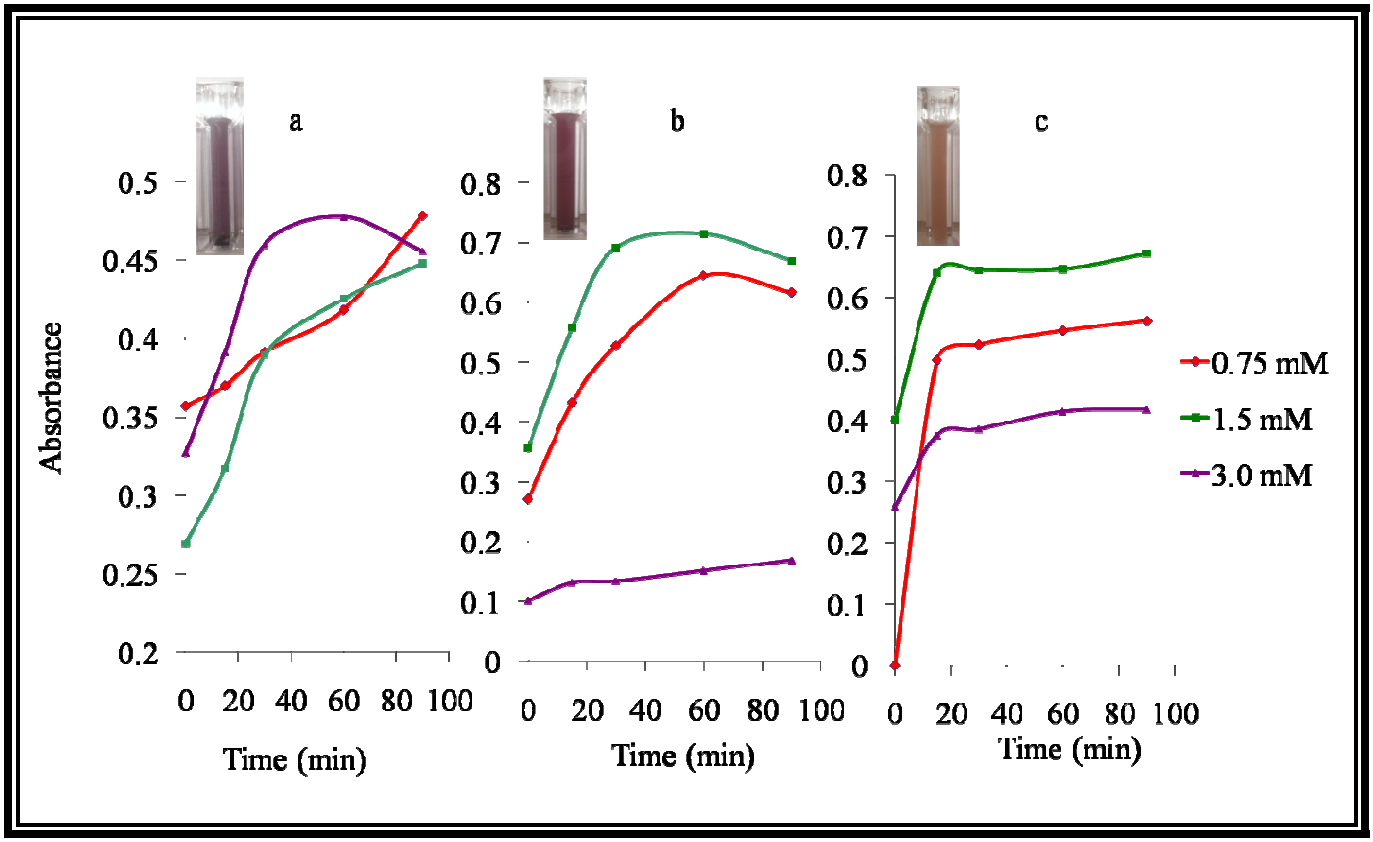

Figure 4.2: Concentration profile for gold nanoparticles biosynthesized by reduction of Au^{3+} in; a) isopropanol alfalfa biomass extracts, b) methanol alfalfa biomass extracts, and c) water alfalfa biomass extracts. Insets show the real-time pictures of the nanoparticles in solution.

The extracts prepared in isopropanol and methanol evidently contained high amounts of chlorophyll as seen by the deep green color of the extracts, while the water extracts did not present that characteristic (pictures not shown). Other secondary metabolites found in methanol and isopropanol extracts include flavones, flavanones, glycosides, and other phenolic derivatives as reported in the literature [25]. By observing the molecules, shown in Illustration 4.1, found in the alfalfa extracts, we can assume that the nanoparticles are being formed by redox chemistry between the organic molecules and the Au^{3+} ions. Furthermore, some of the molecules such as the flavonoids and flavanones having the carbonyl and the hydroxyls in the ortho positions can cap the nanoparticles by chelation. Also, cystein can be acting as both, reducing and capping agent.

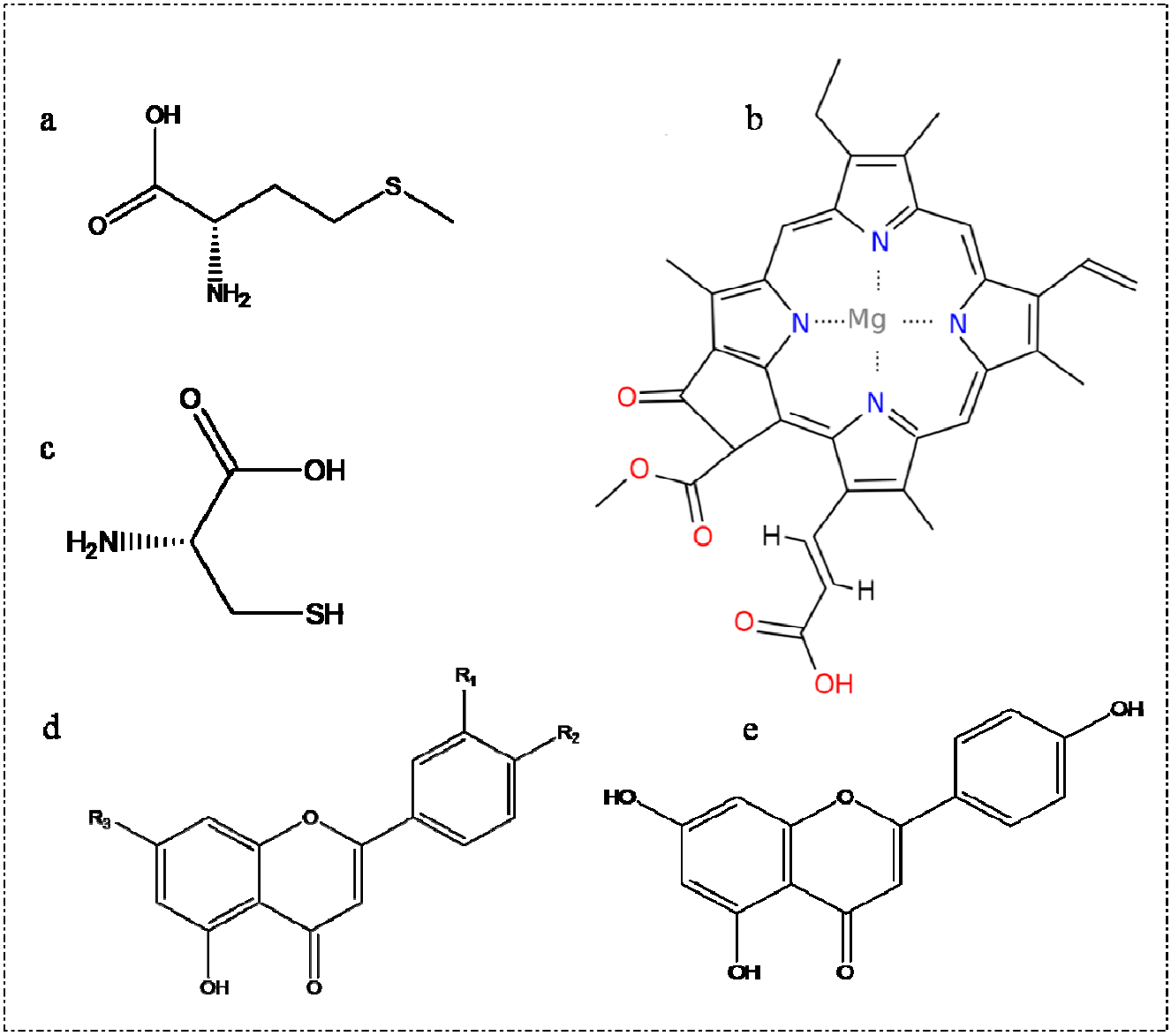

Illustration 4.1: Organic molecules found in alfalfa extracts including a) methionine, b) chlorophyll, c) cystein, d) general structure of flavonoids found in methanol alfalfa extracts, substituents include H, OH and various glucosides, and e) apigenin [25].

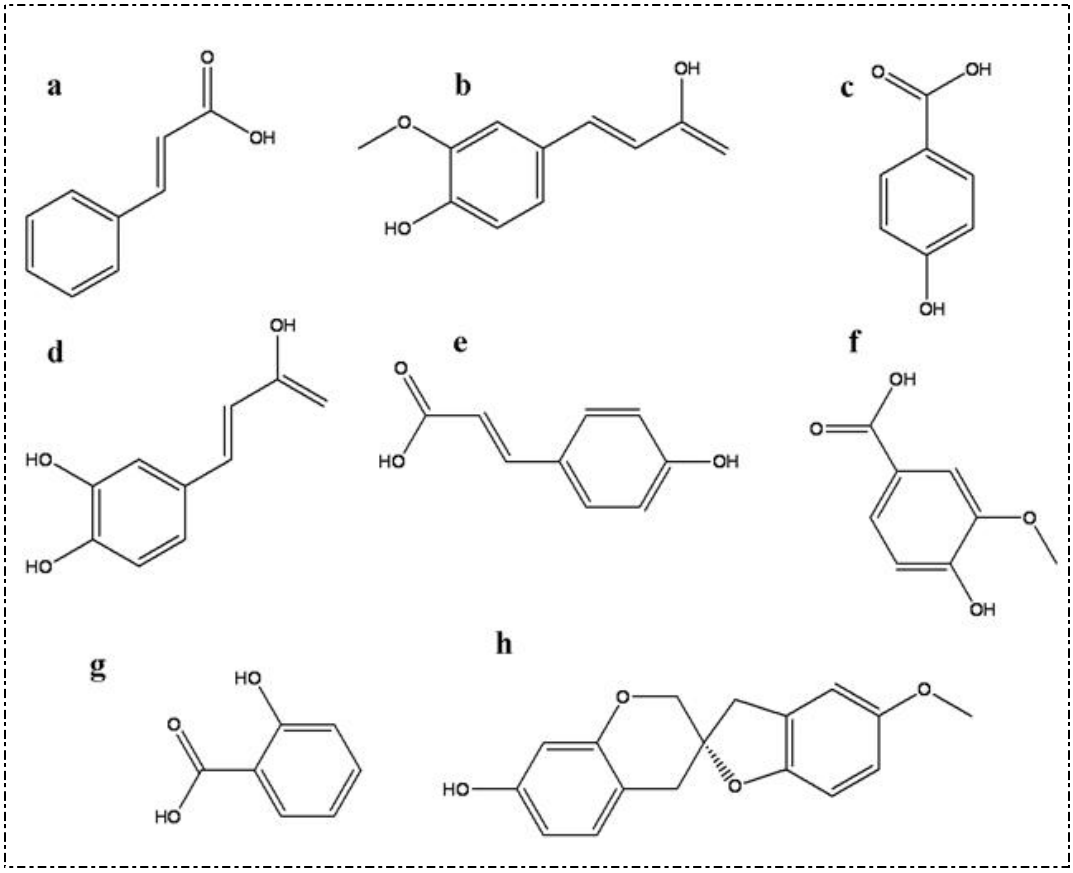

Illustration 4.2: Some of the water soluble compounds found in alfalfa. a) cinnamic acid, b) ferulic acid, c) *p*-hydroxybenzoic acid, d) caffeic acid, e) *p*- coumaric acid, f) vanillic acid, g) hydroxybenzoic acid, and h) medicarpin

According to the literature, alfalfa water extracts include cinnamic acid and its derivatives, hydrobenzoic acid, *p*-coumaric acid, ferulic acid, hydroxybenzoic acid, trans-cinnamic acid, caffeic acid, saponin, and medicarpin [56]. The different compounds found in the extracts when using different solvents, can be the reason for the variations in nanoparticle morphologies found when using alfalfa extracts. As mentioned above, common characteristic of these compounds are their carboxylic acid and hydroxyl moieties, yet in comparison to the extracts in the alcohols, the molecules are small organic acids with the exception of the saponin (Illustration 4.2). The water soluble compounds in the AWE are small molecules that facilitate the reduction of the Au^{3+}. The reduction step in the ABW mixture was slower in the first 10 minutes and the nucleation started occurring almost immediately in the 0.75 mM Au^{3+} as compared to the higher concentrations. This is evident in the absorption spectra in Figure 4.2c, which shows zero absorbance at zero time. Nanoparticle agglomeration occurs faster in the first 15

minutes reaching an absorbance of c.a. 0.5 absorbance units. Increasing the concentration of gold ions in the mixture, increases the rate of reduction considerably (0.4 a.u at time zero), and the nucleation happens in the same fashion as in the lower concentration. Gold ion concentration of 3.0 mM increased the reduction step, but nucleation and growth rate of nanoparticles did not change in 90 minutes of reaction.

In order to understand the reduction of the gold ions from the beginning of the reaction, a continuous kinetics experiment was performed for the reactions of Au^{3+} with ABM and ABW, and the results are shown in Figure 4.3. In these results, it is evident that the reduction of gold ions in ABM is faster in the first few minutes than that of water extracts. As seen in Figure 4.3a, the exponential growth indicates reduction and nucleation occurring in the first 30 minutes, followed by agglomeration and growth. On the other hand, the ABW reacted with the Au^{3+} shows a slower reduction and nucleation (Fig. 4.3b inset), followed by a constant nucleation step during the following 60 minutes. Agglomeration and growth occur at a lower rate, and the growth rate slows down after 4h as it reaches its maximum velocity. The data shown suggests that higher concentration of the gold ions in the reaction mixture is crucial for the reduction of the ion to occur, leading to fast nucleation of gold nanoparticles. It also shows that the nanoparticle formation in the different extracts follows different behaviors and that there is a significant difference in the reactions using alcohols as solvents for the extraction preparation from the reactions where water is used as a solvent. However, this data does not give information about the deposition trend of the nanoparticles which results in different morphologies. For this reason, electron microscopy characterization was used to further study the biosynthesized gold nanoparticles.

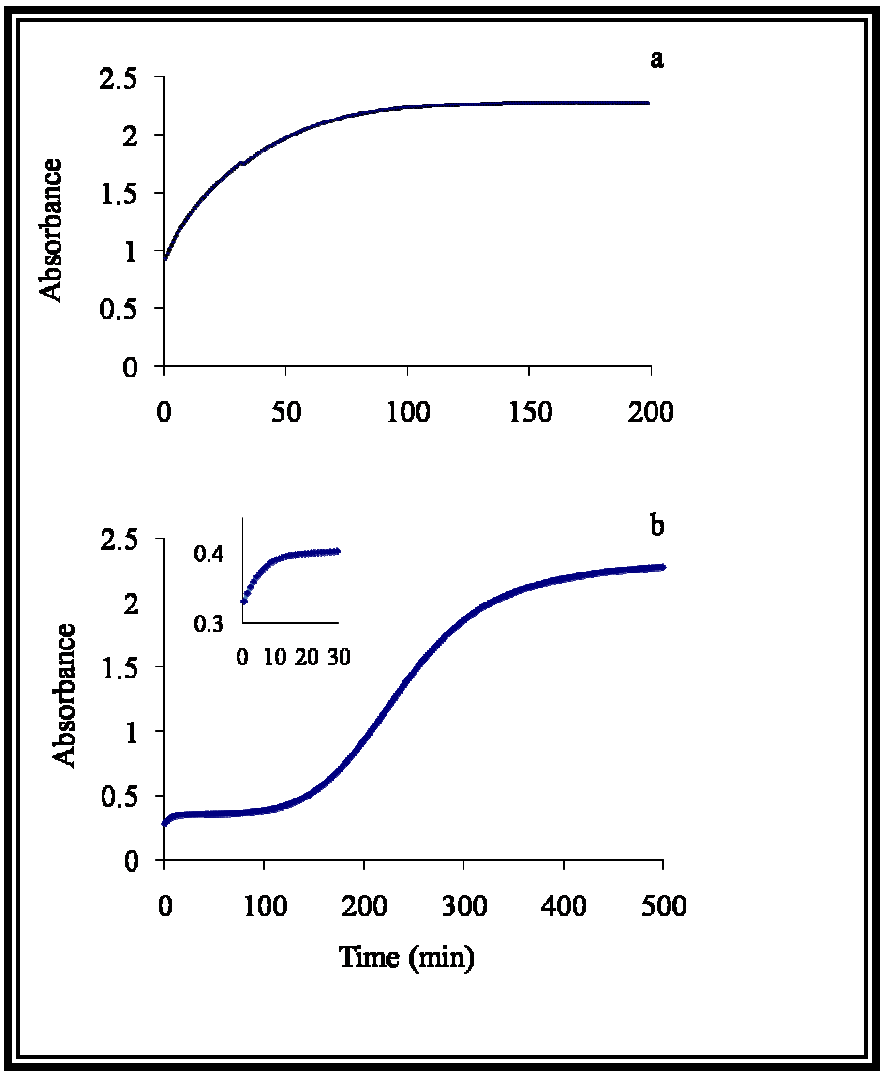

Figure 4.3: UV-Vis spectra of gold nanoplates biosynthesized using: a) methanol alfalfa biomass extracts and b) water alfalfa biomass extracts (inset: absorption spectra in the first 30 minutes).

4.1.3 Nanoparticles biosynthesized using methanol alfalfa biomass extracts

Reduction of Au^{3+} by ABM resulted in the production of monodisperse gold nanoparticles with size range from 10-50 nm. The characteristic purple color of gold nanoparticles in this size range was visible after 15 minutes of reaction (Figure 4.2b). The gold nanoparticles biosynthesized by adding ABM to a 3 mM Au^{3+} solution at pH 2 were observed by SEM as seen in Figure 4.4.This sample was chosen for SEM characterization because according to the kinetics results, the nanoparticles were not agglomerating into larger particles, as seen in figure 4.4, which shows spherical monodisperse

nanoparticles in the range of 50 nm. The solvent effects in the extract preparation are evident in these results. Both CH_3OH and $CH_3CH_2CH_2OH$ are polar organic solvents which are most likely to extract higher concentrations of organic species from the alfalfa biomass than from water, due to their slightly lower polarity. As seen in Figure 4.2 above, the trends of nanoparticle formation in both ABI and ABM are similar, but the size range of the nanoparticles formed in the ABI was slightly broader than those produced in ABM, indicating that ABM facilitates the electron transfer reaction faster than ABI, allowing the nucleation, agglomeration and growth of the nanoparticles to happen almost at the same time from the beginning of the reaction. Thus, gold nanoparticles are able to aggregate in a more monodisperse fashion and grow more freely on ABI than on the ABM extract.

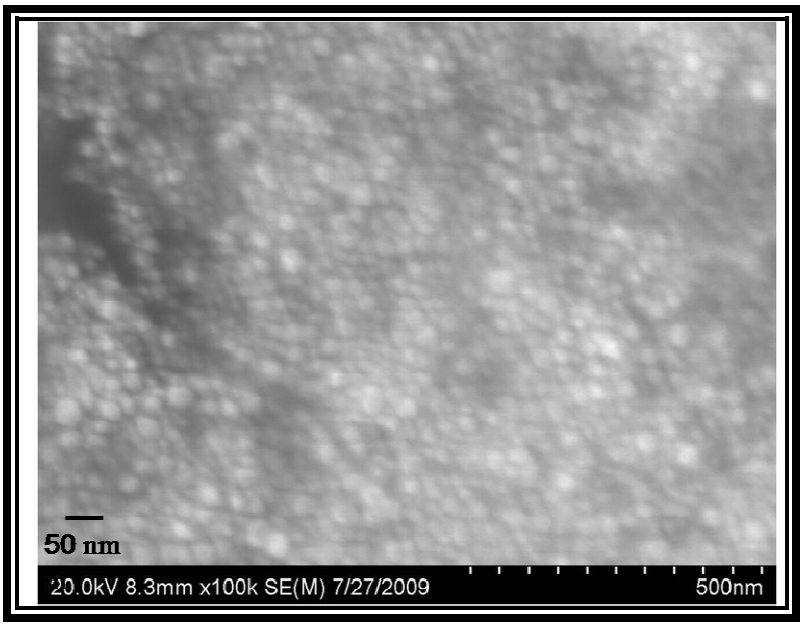

Figure 4.4: SEM image of gold nanoparticles biosynthesized using methanol alfalfa extracts (ABM).

To further analyze the gold nanoparticles in this sample, TEM characterization was performed. Gold nanoparticles of decahedral and icosahedral shapes were found in the biosynthesis using ABM. As seen in Figure 4.5a, size monodispersity was achieved finding gold nanoparticles from 20-50 nm in diameter and some smaller nanoparticles, which are considered gold seeds and can be removed from the sample by centrifugation. The sample was taken after 1h of reaction, and Figure 4.5b shows the agglomeration of one seed onto another that appears to be a decahedral nanoparticle. Figure 4.5c shows

a spherical seed merging onto an icosahedral gold nanoparticle, representing the growth stage of the nanoparticle formation, thus corroborating the results obtained from the kinetic data shown in the previous section (Figure 4.3b). A high resolution image of a gold nanoparticle can be seen in Figure 4.5d, which appears to be a truncated icosahedrons in the (001) orientation [57].

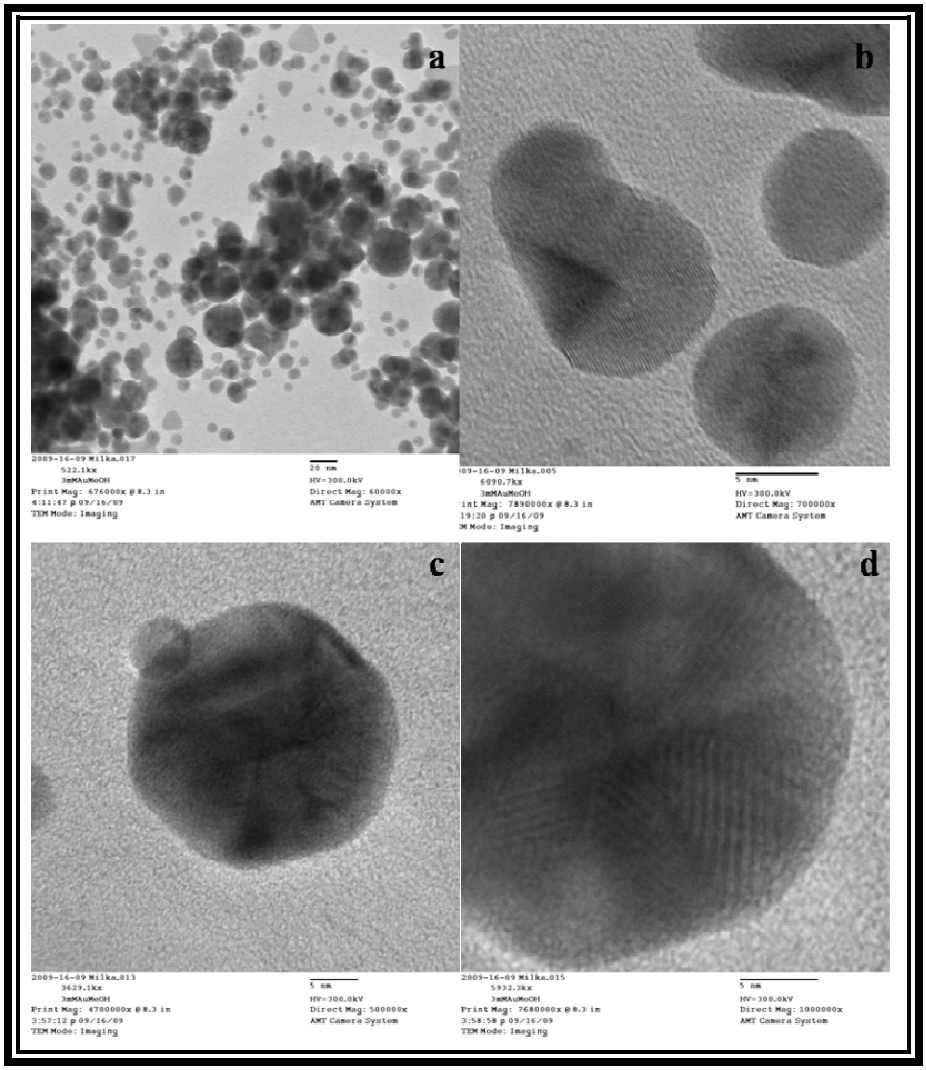

Figure 4.5: TEM images of gold nanoparticles biosynthesized in MAE: a) gold nanoparticles produced in ABM showing size monodispersity, b) close up image of a decahedral and an icosahedral gold nanoparticle c) icosahedral gold nanoparticle showing growth, and d) high resolution image of an icosahedral gold nanoparticle

4.1.4 Characterization of gold nanoparticles biosynthesized using isopropanol alfalfa biomass extracts

Biosynthesis of gold nanoparticles by reduction of the tetrachloroaurate ion ($AuCl_4^-$) was visible to the naked eye after 1h of reaction with the alfalfa extracts in isopropanol. The characteristic purple color was visible for a few seconds, followed by a darker bluish purple. UV-Vis spectra show a broad plasmon absorption band at 539, nm which is characteristic of gold nanoparticles (Figure 4.6b). The peak symmetry and sharpness indicates the anisotropy of the gold nanoparticles, as compared to spectral data obtained with other plant extracts [34, 58]. For instance, gold nanoparticles synthesized using geranium leaf extracts showed an absorption band between 547 and 551 nm [34]. The size and shape of gold nanoparticle biogenesis can be controlled by pH variations, and in previous reports, the highest percent of gold bound to oat biomass and forming gold nanoparticles was at pH 3 and 5 [10]. In the present work, polyhedral nanoparticles were formed in the reaction mixture consisting of alfalfa biomass extracts in isopropanol and 3mM Au^{3+} solution at a pH of 3.0, with an average size of 25-50 nm as seen in Figure 4.6a.

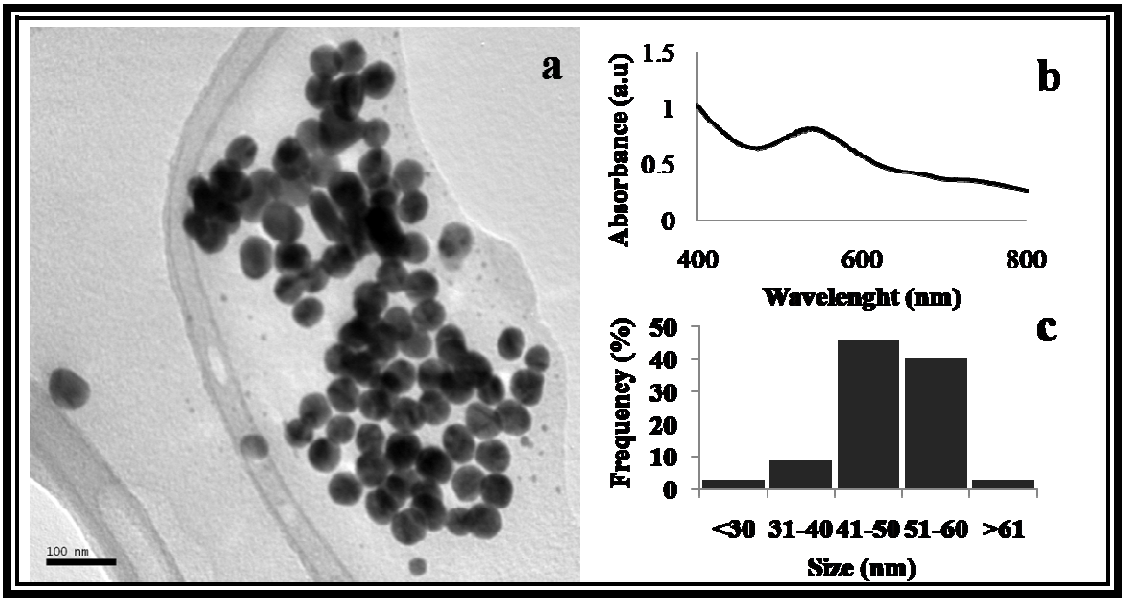

Figure 4.6: Gold nanoparticles biosynthesized using isopropanol alfalfa biomass extracts: a) TEM image of gold nanoparticles, b) UV-Vis spectra of gold nanoparticles, and c) size distribution of gold nanoparticles (n=70).

Reduction of Au^{3+} was tuned by inactivated alfalfa biomass extracts using isopropanol as the solvent in the preparation of the extract. The reducing activity of alfalfa extracts is attributed to its high content of phenolic compounds, including flavonoids as well as its high protein content [27]. It has been established that extracts of different plant species produce distinct sizes and shapes of nanoparticles. This observable fact occurs as a result of the presence of functional groups such as carboxyl (–COOH), amino ($–NH_2$), and sulfhydryl (–SH). Distinctly, varying the solvents used in the extraction procedure yields different shapes and sizes of gold nanoparticles within the same plant species [36].

In the present study, polyhedral gold nanoparticles were succesfully separated from larger gold nanoparticles by sonication and centrifugation. The morphologies observed in the sample were decahedral gold nanoparticles (Figure 4.7) of about 30 nm and gold icosahedra. The decahedra lay onto the faces showing a five-fold symmetry, where the particle is divided by 5 twin interfaces (Figure 4.7a). The fast fourier transform (FFT) taken on top of the twin boundary shows a double diffraction, attributed to the defect created on the two adjacent tetrahedral units (Figure 4.7b and 4.7c). Figure 4.7d shows another decahedral gold nanoparticle of ~30 nm in diameter. As with the previous one, it presents a five fold symmetry marked by twin planes. Weak beam dark field (WBDF) was carried out using the (220) spot. In this mode the tetrahedra forming the particles are more easily identified as the defects are highlighted.

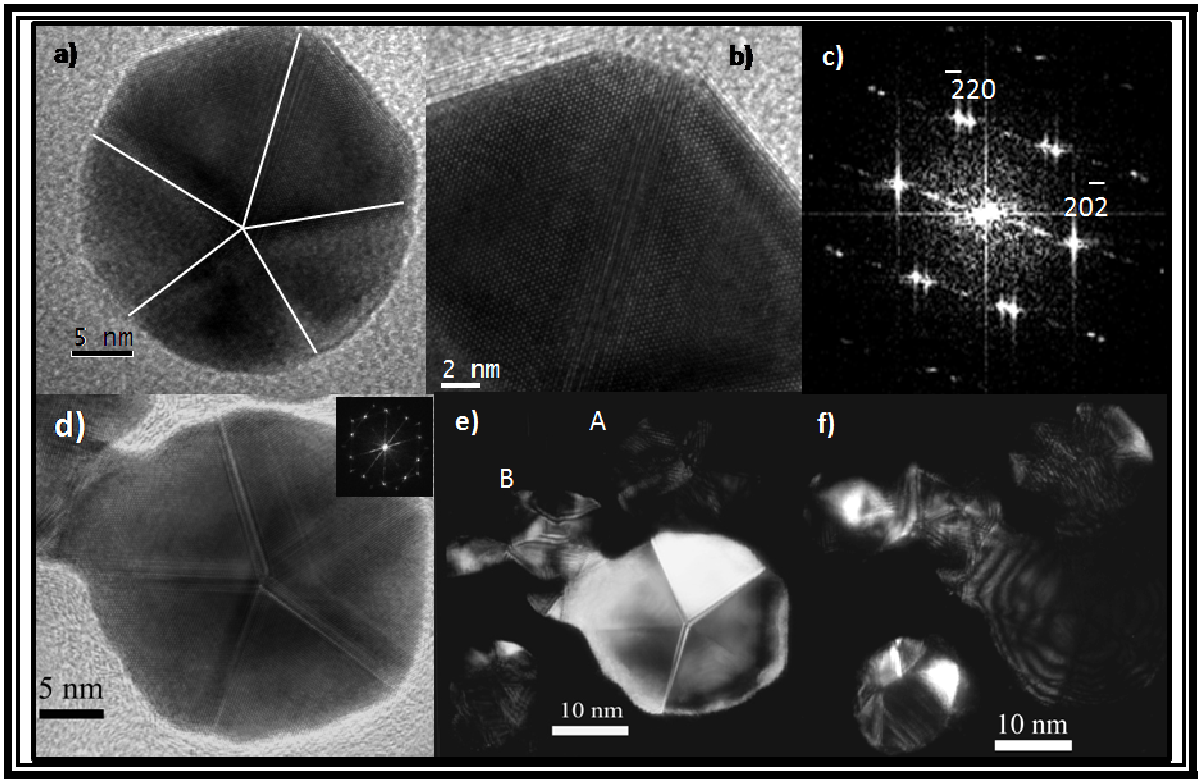

Figure 4.7: TEM images of a gold nanoparticcles: a) decahedron where five defects are marked with lines, b) HRTEM image recorded along the [111] orientation, c) FFT indexed assuming *Fm*-3*m* symmetry, d) HRTEM image of a different decahedron perfectly tilted perpendicular to the electron beam, the FFT is shown inset, e) High resolution WBDF image recorded at 0°, and f) high resolution WBDF image taken of the sample tilted 5 degrees.

Under certain tilting angles, the tetrahedra present more or less brightness when it obeys the Bragg condition, as shown in Figure 4.7e. In this image, gold icosahedra marked as A and B are also present. In the case of A, the icosahedron is observed from a top view exhibiting a five fold symmetry. Meanwhile, B presents a typical butterfly image [59]. Contour lines representing the thickness of the decahedron were observed by tilting the sample several degrees (Figure 4.7f).

Icosahedra of about 25-30 nm in diameter were found together with the decahedra in the sample. Figure 4.8a shows a bright field image of one of the icosahedra. A close up image of it is displayed in Figure 4.8b, where Moire fringes appear due to the superposition of the tetrahedra assembling the particle. The distance measured between those fringes was found to be 0.61 nm. Meanwhile, the lattice

distance between planes was 0.24 nm . The calculated distance between Moire fringes was 0.39 nm according to the equation shown below. The calculated theoretical values for d_{111} and d_{220} were approximately 0.37 nm.

$$D = d1 \cdot d2 / | d1 - d2 |$$

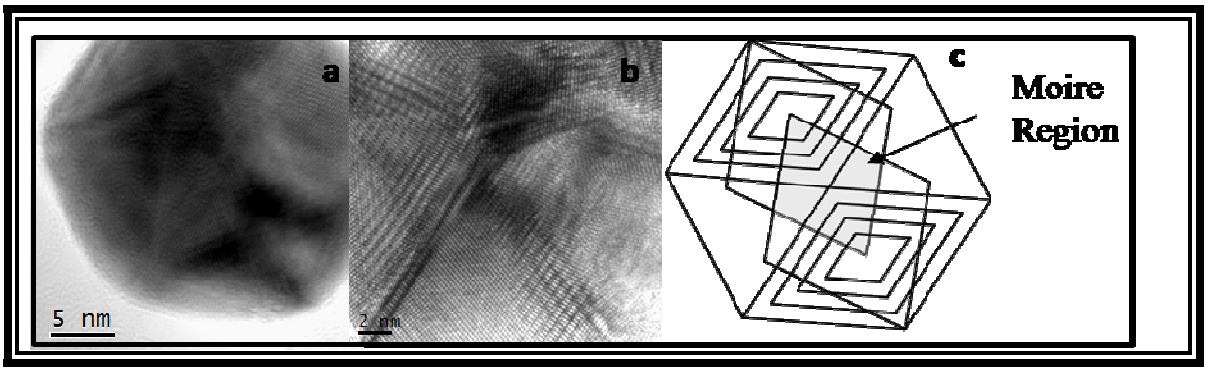

Figure 4.8: a) Bright field TEM image of a gold tetrahedron, b) HRTEM image of the icosahedra, where Moire fringes are observed in the figure, and c) schematic representation of the tetrahedron observed.

4.1.5 Nanoplates biosynthesized using water alfalfa biomass extracts

Gold nanoplates were biosynthesized by inactivated alfalfa biomass extracts prepared in water. The shapes of the nanoplates were hexagons, truncated triangles, and triangles, the triangular faces being the most abundant (Figure 4.8). Reduction of $AuCl_4^-$ by the extracted compounds in the alfalfa extract was evident and monitored by UV-Vis spectrophotometry. Figure 4.2 shows the time profile of nanoparticle formation and its growth as the reduction of the tetrachloroaurate ion takes place in the presence of reducing agents in the alfalfa extract. As seen in the figure, reduction of the Au^{3+} ion takes place immediately after adding the reducing agents to the solution, followed by a rapid increase in the absorbance which reaches a plateau. After 2 h of reaction, the absorbance starts increasing exponentially reaching the maximum after 4 h.

The solution starts changing color from a pale pink to a muddy brown, after 12 h of reaction, indicating the formation of the gold nanoplates (Figure 4.2c inset). Previous studies have shown that gold nanoplates synthesized via humic substances absorb at 910 nm [60]. Since the absorption of gold nanoplates was out of range in the instrument used (Cary 20), there is no spectrophotometric data; however, the formation of the nanoplates was observed by scanning electron microscopy and transmission electron microscopy. Figure 4.8 shows the image of a sample taken after 12 h of reaction. Shape control was achieved during the synthesis by using the different solvents in the preparation of the alfalfa extracts. As previously stated, in the case of the gold plate formation, the extracts were prepared with water (ABW). Although smaller particles were also present in this sample after the synthesis, they were successfully removed by ultrasonic treatment and size selective precipitation.

In Figure 4.9, there is a clear indication that the majority end-product of the reaction of Au^{3+} with alfalfa extracts in H_2O are monodisperse gold plates of three different shapes (Figure 4.9a and b), as opposed to the monodispersed icosahedral and decahedral nanoparticles found in the ABI (Figures 4.4, 4.6, and 4.7).

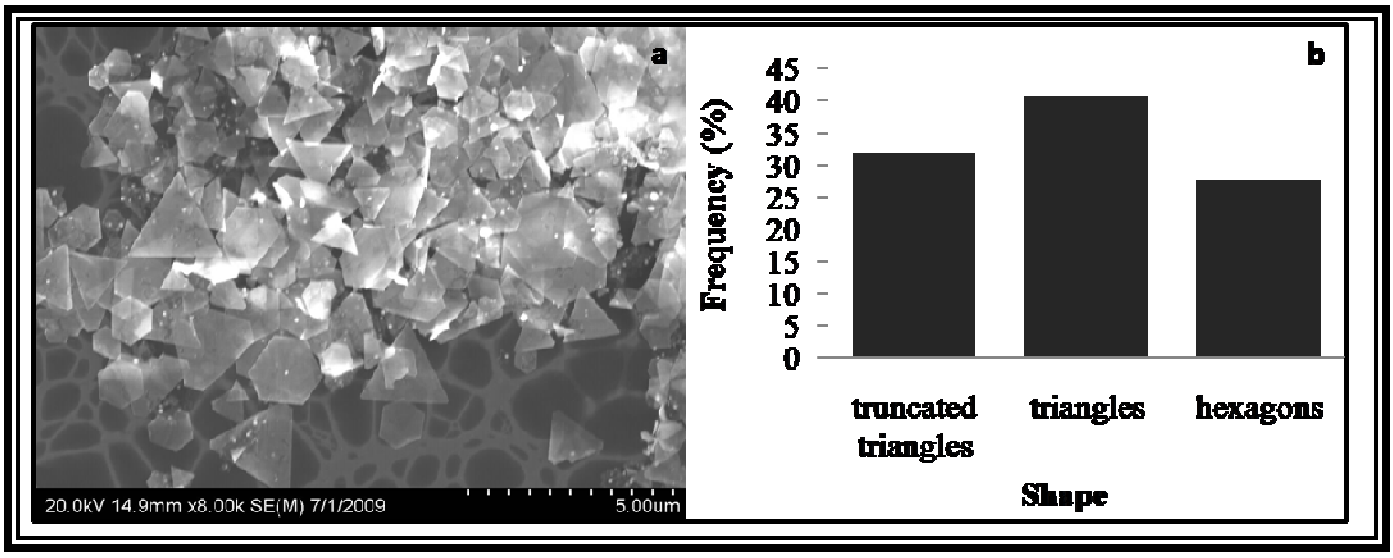

Figure 4.9: Gold nanoplates biosynthesized using H_2O alfalfa biomass extracts, a) SEM image of gold plates of different morphologies, b) morphology distribution, n=47.

High resolution SEM (HRSEM) and AFM were also used in the characterization of the gold plates. As seen in Figure 4.10a, HRSEM micrographs show the different morphologies of the plates ranging from 500 nm to 4 μm in length; thickness was measured on particles which lay more parallel to the electron beam (Fig. 4.10b), obtaining values of 15 to 30 nm, which was confirmed by AFM analysis. A closer observation of the crystals revealed certain roughness on the surface (Fig. 4.10b inset). The formation of the triangular crystals is attributed to the accelerated growth in certain directions of the hexagons, which evolve to the final morphology through the formation of truncated triangles, and as a consequence, the twin planes run along the entire crystals [61].

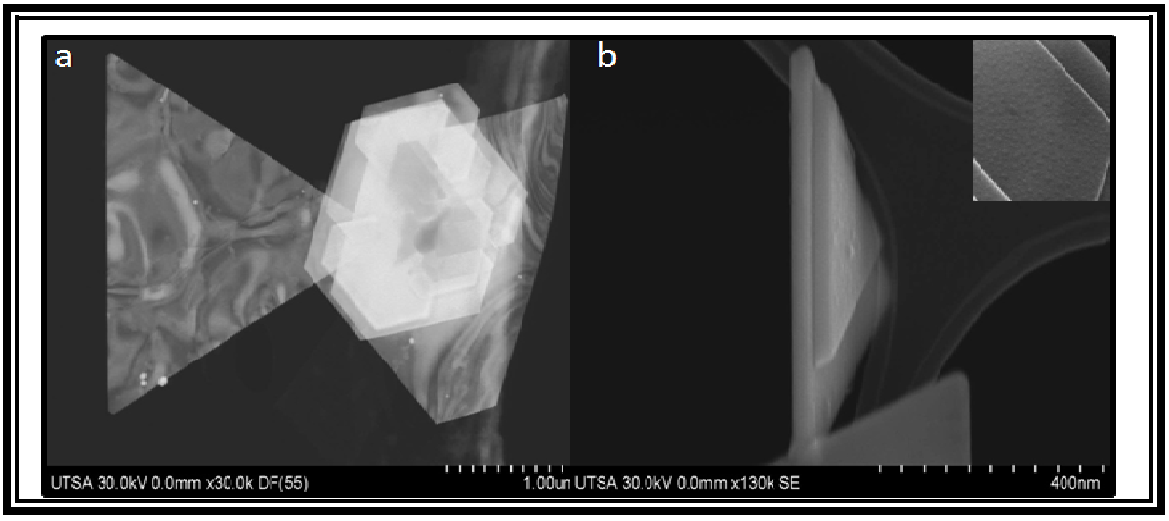

Figure 4.10: a) HRSEM images of synthesized product showing different morphologies. b) Two triangles tilted several degrees where the thickness of the crystals can be measured. A higher resolution image of the surface of one of the crystals is shown inset.

Figure 4.11 shows the tapping mode AFM images of the Au triangular plates on a 500 × 500 nm scan area. The dimension of one of the sides of the triangle observed in this image was up to 500 nm in length. The height profile analysis of the Au plate indicates that the thickness of the Au in this case was between 20-25 nm, further confirming the monodispersity of the plates [60].

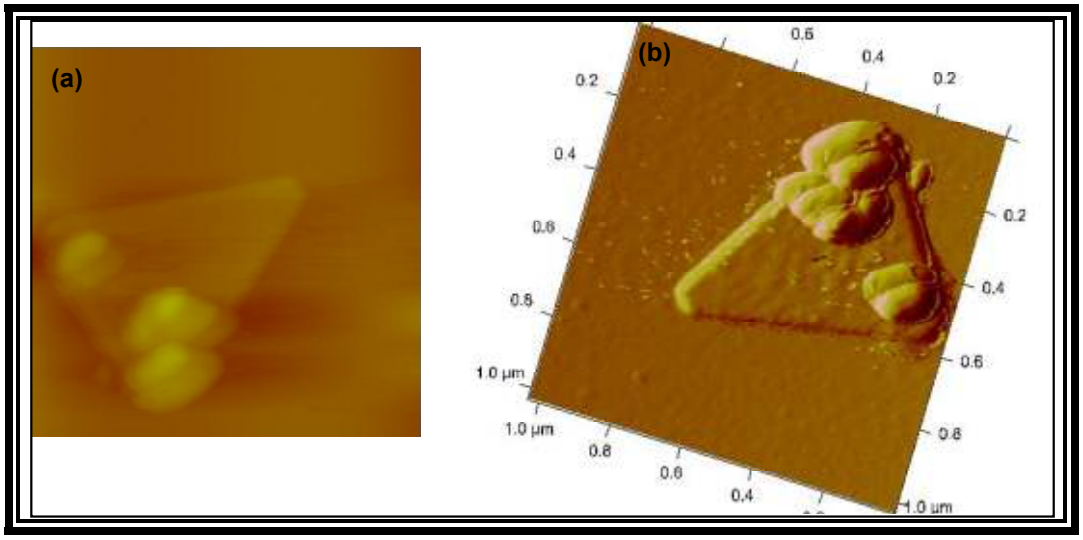

Figure 4.11: a) Tapping mode AFM image of the Au triangles (500 × 500 nm scan area), b) 3-D image of the Au triangle. (The images in the scans show a 1×1 µm area).

TEM analysis was carried out to study the structure of the particles (Figure 4.12). High resolution TEM (HRTEM) confirmed a single crystal structure in the entire surface of all the plates (Figure 4.12b) where no defects were present. The SAED corroborated the single crystal structure (Figure 4.12b) and was indexed assuming *fcc* structure along the [111] orientation, obtaining a unit cell value of a = 4.080 Å. Forbidden reflections commonly observed in similar gold and silver nanoparticles [61-64] have been indexed as 1/3{422} with a lattice distance of 0.25 nm. The different contrast observed in the WBDF mode using the forbiden reflections (Figure 4.12c), is attributed to the bending ocurring to such large and thin materials. The fact that no dislocations or defects were observed in the nanoplates suggests that the forbidden reflexions were produced by defects running parallel to the (111) plane. The production of these spots has been widely disscussed [64] and they can also be attributed to the arising of the first Laue zone or to the fact that the crystal has a number *n* of s layers where *n*=1mod(3) or *n*=2mod(3). However, the presence of truncated triangles and triangles suggests the presence of stacking faults running parallel to the (111) surface, enclosed by atomic layers on top and

bottom, and bound by {111} planes, which might be the ultimate reason for the existence of the extra spot [65-68].

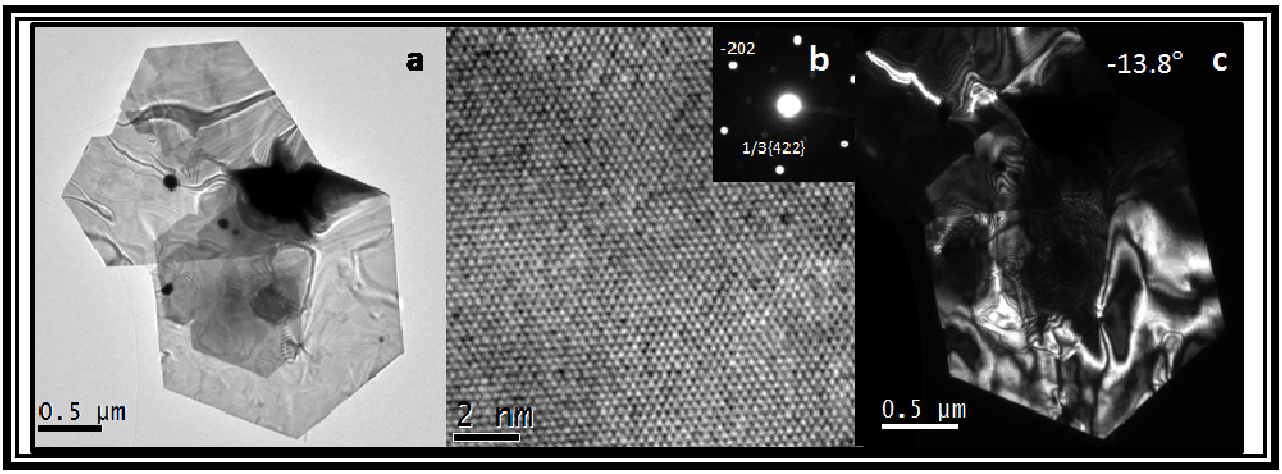

Figure 4.12: a) Low Magnification TEM image of gold nanoplates, b) HRTEM image recorded on top of the hexagonal plate, SAED pattern of the nanoplate indexed assuming $Fm\bar{3}m$ symmetry is shown inset, c) WBDF images obtained using the 1/3{422} spot of the sample tilted -13.8° in the α angle.

4.2 Chemical and Physical Extractions of Gold Nanoparticles from Alfalfa Biomass

4.2.1 Solvent extraction of gold nanoparticles from alfalfa biomass

Powder alfalfa biomass was used as a reducing environment for Au^{3+} in order to test the hypothesis that the nanoparticles could be recovered from the biomass using chemical and physical extractions. Previous studies had shown that oat and wheat biomasses' functional groups such as carboxylic acids, amines and thiol act as reducing and binding agents for gold [38]. In the attempt to maximize the recovery of gold nanoparticles from alfalfa biomass, H_2O, H_2SO_4, NaCl, and TritonX were used as extractants. Figure 4.13 shows the UV-Vis spectra of the supernatants, which contained the recovered nanoparticles. The characteristic absorption band c.a.530 nm can be observed in all the extracted nanoparticles. However, the NaCl and H_2SO_4 efficiency was lower than the Triton X and water, in that order. Sodium chloride in solution and sulfuric acid did not extract many nanoparticles from the biomass. On the other hand, the surfactant Triton X extracted more nanoparticles that might

have hydrophobic groups attached and are easily broken from the biomass. Water was the most efficient of the extractants, recovering most gold nanoparticles from the biomass of similar size as it can be seen by the sharper absorption band.

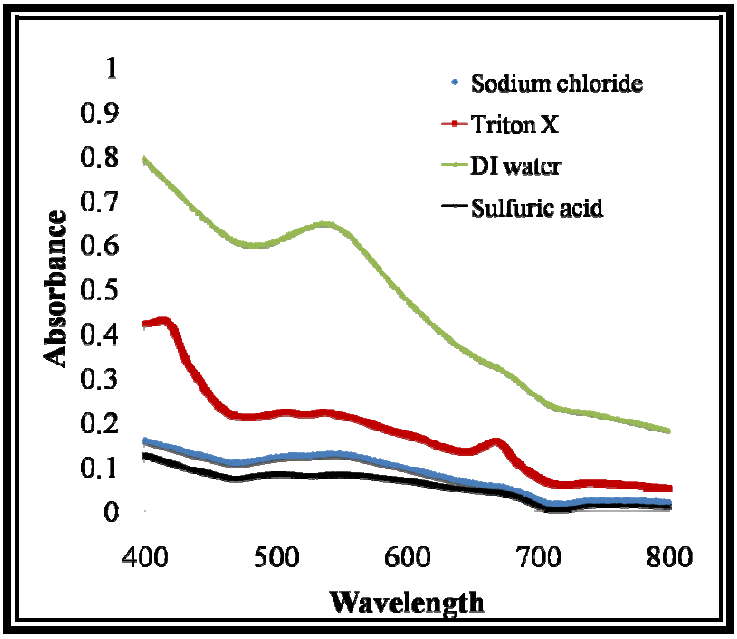

Figure 4.13: UV-Vis spectra showing the efficiency of extracting gold nanoparticles from alfalfa biomass using different solvents.

In order to further evaluate the efficiency of the extractions, the biomass was analyzed by x-ray diffraction after being washed with the solvents. X-ray diffraction patterns (diffractograms) of amorphous materials such as nanoparticles show broad peaks due to the lack of crystallinity in the sample. The diffraction pattern of crystals has sharp peaks that correspond to various crystal planes that necessarily have a long range order, as shown in the instrumental section, and explained by Bragg's law. On the other hand, amorphous solids and liquids do not have the same long range order than crystals do, yet since the atoms in the amorphous solid are tightly packed, the atomic distances have a narrow distribution and the intensity of the scattered x-rays forms a maxima with a wide distribution [11]. Figure 4.14a shows the typical x-ray diffractogram of crystalline fcc (face centered cubic) Au, and Figure 4.14b shows that of the gold nanoparticles embedded in the biomass. As seen by the differences

in the diffractograms, after solvent extraction (shown above), more nanoparticles were still found in the biomass.

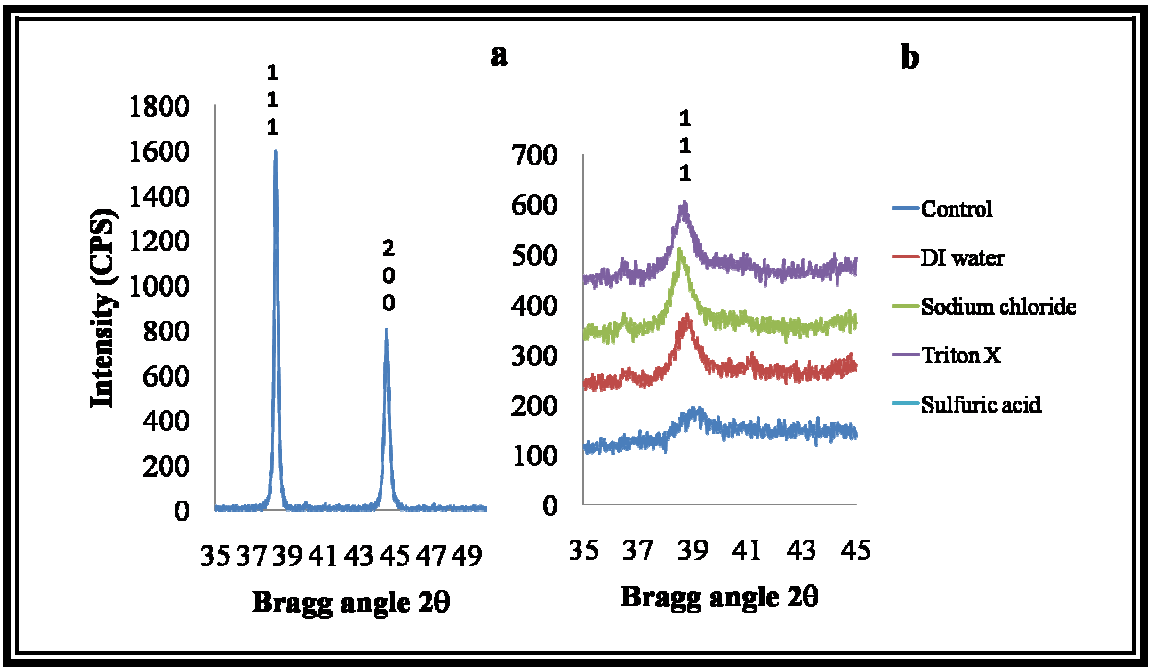

Figure 4.14: X-ray diffraction pattern: a) crystalline gold, and b) gold nanoparticles in alfalfa biomass after solvent extraction.

The diffraction peaks at 38.5 degrees in the 2θ axis are those corresponding to the first line of gold corresponding to the (111) lattice plane and the average nanoparticle size was of 14 nm, as calculated from the full witdh half maxima (FWHM) of the peak and using Scherrer's equation (Equation 3).

4.2.2 Physical extraction of gold nanoparticles from alfalfa biomass

Another approach to the recovery of gold nanoparticles from the alfalfa biomass was through pyrolysis of the organic matter in the alfalfa biomass. The biomass containing the gold nanoparticles was incinerated at different temperatures to dispose of the organic material through its conversion to CO_2 and the remaining gold nanoparticles were analyzed by X-ray fluorescence and X-ray diffraction. Pyrolysis of hemicellulose, cellulose and lignin occur at 250°C-500°C [69]; for this reason, the

temperatures chosen to extract the gold nanoparticles were in the range of 400°C to 600°C. Figure 4.15a shows the X-ray fluorescence spectra of the gold standard, and Figure 4.15b shows the alfalfa biomass before and after nanoparticle biosynthesis. XRF spectra of the alfalfa biomass with the gold nanoparticles before and after pyrolysis is shown in Figure 4.15c. The XRF spectra show the difference between alfalfa biomass without gold, and after gold addition and nanoparticle biosynthesis.

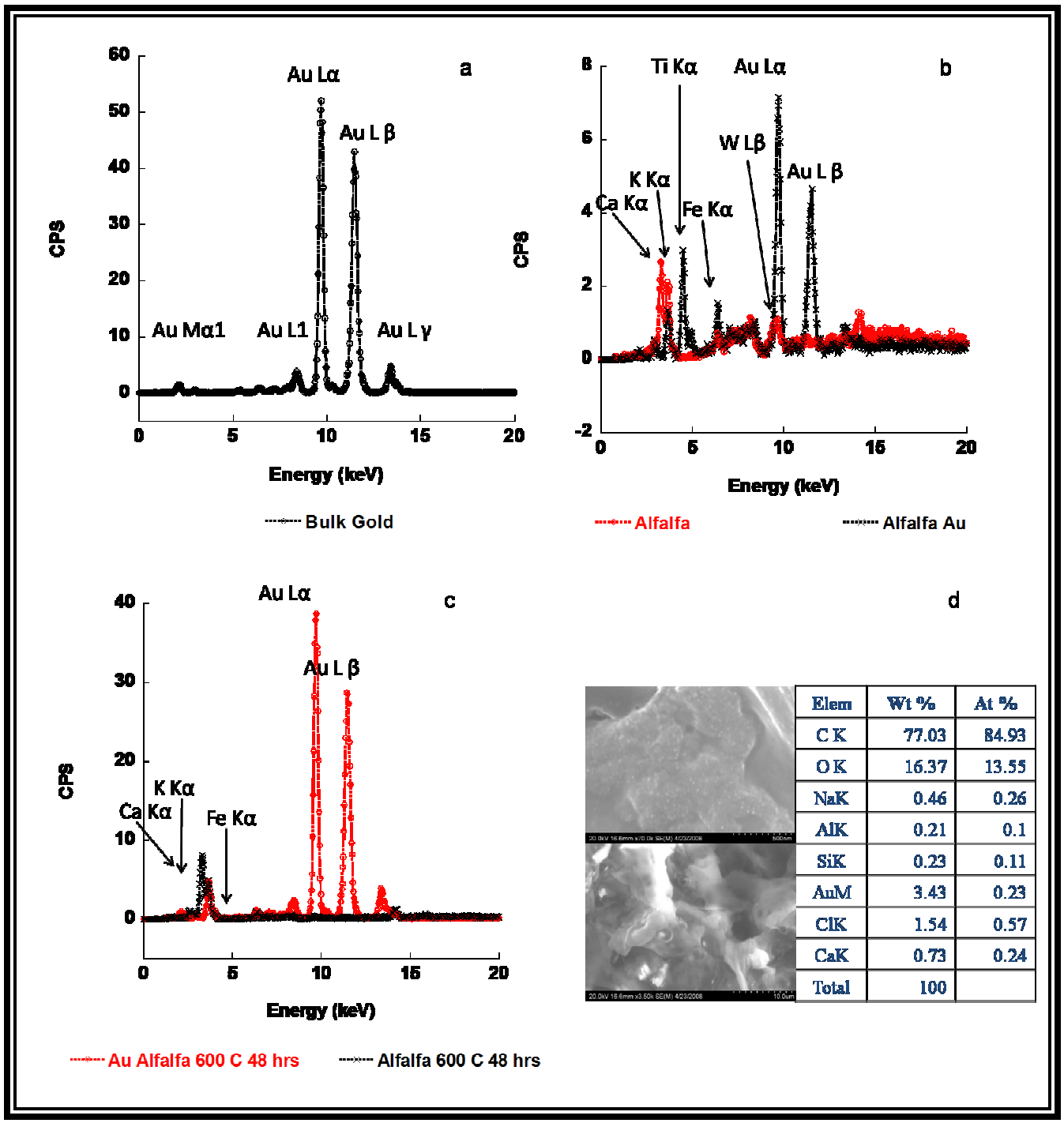

Elem	Wt %	At %
C K	77.03	84.93
O K	16.37	13.55
NaK	0.46	0.26
AlK	0.21	0.1
SiK	0.23	0.11
AuM	3.43	0.23
ClK	1.54	0.57
CaK	0.73	0.24
Total	100	

Figure 4.15: X-ray fluorescence spectra of a) bulk gold, b) alfalfa and alfalfa with gold nanopartilces, c) alfalfa with gold nanoparticles after pyrolysis, and d) SEM image with EDAX analysis of alfalfa biomass before pyrolysis.

These results are also seen in the SEM image (Figure 4.15d) and the EDAX shows the presence of gold in the samples. After the pyrolysis of the biomass, the gold nanoparticles were left behind in the

sample, even at the highest temperature since the melting temperature of gold nanoparticles is 830°C and that of bulk gold is 1350°C. Although the pyrolysis of the organic material in the biomass was successful, the recovered gold nanoparticles lost their properties. As seen in the X-ray diffractogram shown in Figure 4.16, the diffraction pattern was that of crystalline gold instead of amorphous solids (in this case gold nanoparticles). Applying high temperatures to the alfalfa biomass containing the gold nanoparticles successfully removed all the organic material, at a high energy cost, for the purposes of this investigation. Gold nanoparticles when exposed to high temperatures resulted in bulk gold due to the agglomeration of the nanoparticles in the sample and the increased attraction forces between particles.

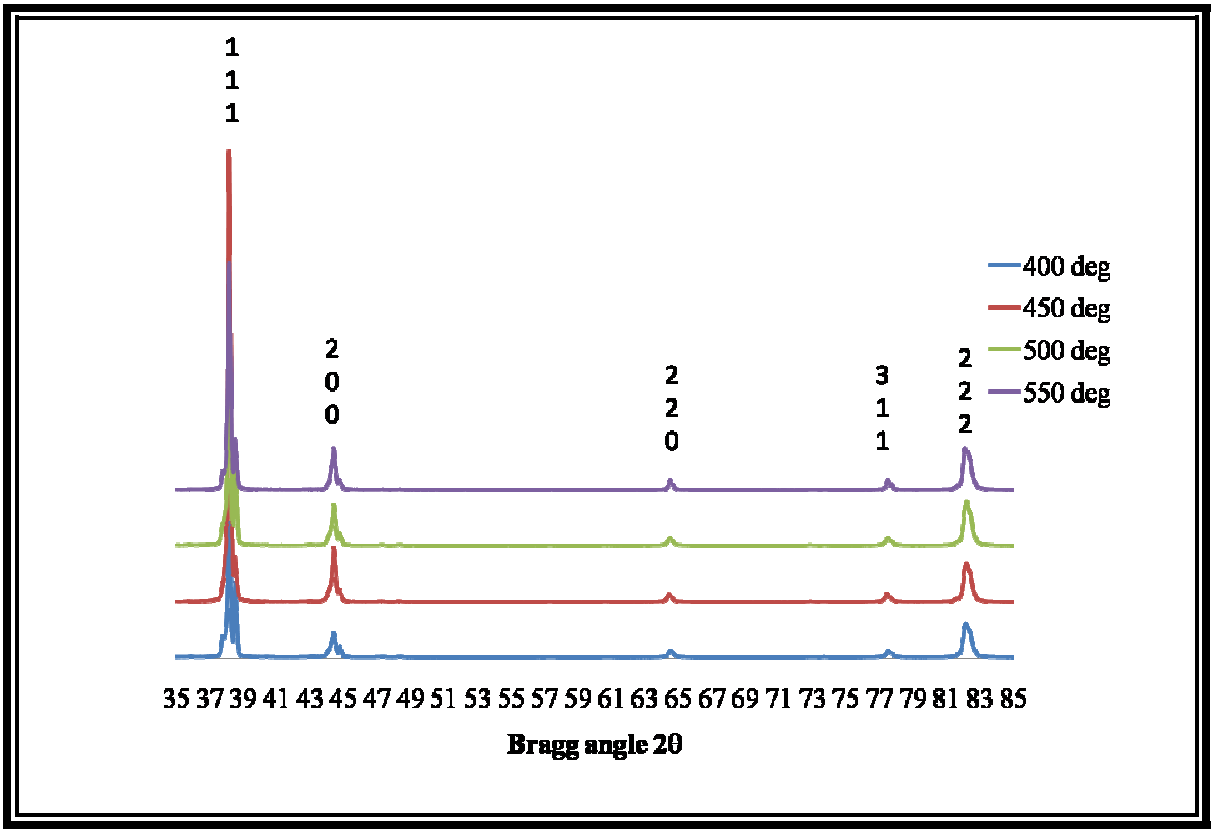

Figure 4.16: X-ray diffraction of gold nanoparticles embeded in alfalfa biomass exposed to pyrolysis at different temperatures.

Chapter 5: Conclusions

The goal of this research was to develop a green and environmentally friendly methodology for the production of gold nanoparticles, as well to investigate the possibility of extracting the gold nanoparticles from alfalfa biomass. The accomplishments of this research are summarized as follows:

A) For the first time, the biosynthesis of gold nanoplates and polyhedral gold nanoparticles was carried out using inactivated alfalfa biomass extracts. Size and shape were controlled by using different solvents during the extract preparation under pH control. To our knowledge, the production of gold nanoplates by alfalfa has never been reported before.

B) Gold decahedra and icosahedra were the most abundant nanoparticles in the isopropanol extract of about 15-60 nm in diameter with low surface energy, lying onto the (111) lattice plane.

C) Gold decahedra and icosahedra of 20-50 nm in diameter also lying on the (111) lattice plane were biosynthesized by Au^{3+} reduction using methanol alfalfa extracts. The gold nanoparticles biosynthesized in the methanol alfalfa extracts showed to be monodispersed and their formation was highly dependent on the pH.

D) Gold nanoplates were biosynthesized by using water alfalfa extracts and the most abundant gold nanoplates were triangular with a size ranging from 500 nm to 4 μm, and a thickness of 20-25 nm, also lying onto the (111) lattice plane.

E) Gold nanoparticles were extracted from alfalfa biomass by using different solvents. The best recovery was achieved by using DI water, and the average size of the nanoparticles in the biomass was of 14 nm, as calculated from X-ray diffraction patterns and Scherrer's equation.

F) The physical recovery by pyrolysis of the organic matter of the biomass resulted in agglomeration of the nanoparticles, and the diffraction patterns of the samples after biomass

pyrolysis had a longer range of crystallinity than before, indicating that the nanoparticles had grown into more ordered crystals.

Overall, these results have proven our hypothesis to be valid; that is, that some natural compounds found in alfalfa biomass act as reducing agents and can be used to develop green methods for the production of gold nanoparticles as an alternative to traditional and more harmful methods. Also, because of the monodispersity observed in the gold nanoparticles and gold nanoplates, it is recommended that further investigation into the applications of these nanoparticles is conducted. In addition, future work should be aimed to characterize the alfalfa extracts and to test the pure compounds to achieve an even more anisotropic gold nanoparticles and gold nanoplates while using a green method for their production.

References

1. Banin U., Millo, O. *Properties*, in *Nanoparticles: from theory to application*, G. Schmid, Editor. 2004, Wiley-VCH.

2. Schmidt, O.G., Deneke, C., Manz, Y. M., Müller, C. Physica E, 2002. 13: p. 969-973.

3. Jain, K.K. Clin Chim Acta, 2005. 358: p. 37-54.

4. Joo, J., Pietryga, J. M., McGuire, J, A., Jeon, S., Williams, D. J., Wang, H., Klimov, V. I. J. Am Chem Soc, 2009. 131: p. 10620-10628.

5. Liong, M., Jie.L., Kovochich, M., Xia, T., Ruehm, S. G., Nel, A. E., Tamanoi, F., Zink, J. I. ACS Nano, 2008. 2: p. 889-896.

6. Anastas, P.T., Williamson, T. C. *Frontiers in green chemistry*, in *Green Chemistry Frontiers in Benign Chemical Syntheses and Proceses*, P.T. Anastas, Williamson, Tracy C, Editor. 1998, Oxford University Press.

7. Anastas, P.T., Warner, J C, *Green chemistry: theory and practice*. 1998, New York: Oxford University Press.

8. Bao, Y., Zhong, C., Vu, D. M., Temirov, J. P., Dyer, R. B., Martinez, J. S. J Phys Chem C, 2007. 111: p. 12194-12198.

9. Johnson, C.J., Dijardin, E., Davis, S. A., Murphy, C. J., Mann, S. J Mater Chem, 2002. 12: p. 1965-1770.

10. Armendariz, V., Herrera, I., Peralta-Videa, J. R., Jose-Yacaman, M., Troiani, H., Santiago, P., Gardea-Torresdey, J. L. J Nanopart Res, 2004. 6: p. 377-382.

11. He, B.B., *Two-dimensional X-ray diffraction*. 2009, Hoboken: John Wiley & Sons.

12. Yang. H., Huang, X. Carbohydr Res, 2004. 339: p. 2627-2631.

13. Ozin G., Arsenault, A. C., Cademartiri L., *Nanochemistry: A chemical approach to nanomaterials*. 2nd ed. 2009, Cambridge: RSC Publishing.

14. Turkevitch, J., Stevenson, P. C., Hillier, H. J. of Phys Chem, 1953. 57: p. 670-673

15. Medley, C. D., Smith, J. E., Tang, Z., Wu, Y., Bamrunsgap, S., Tan, W. Anal Chem, 2008.

16. Huang, L., Guo, Z. R., Meng W., Gu, N. Chin Chem Lett, 2006. 17(10): p. 1405-1408.

17. Vilchis-Nestor, A.R., Sanchez-Mendieta, V., Camacho-Lopez, M. A., Gomez-Espinosa, R. M., Camacho-Lopez, M. A., Arenas-Alatorre, J. A. . Mat Lett, 2008. 62: p. 3103-3105.

18. Harris, N., Ford, M. J., Mulvaney, P., Cortie, M. B. Gold Bull, 2008. 41(1): p. 5-14.

19. Bhumkar, D. Joshi, H., Sastry, M., Pokharar, V. Pharm Res, 2007. 24(8): 1415-1426.

20. Baptista, P., Doria, G., Henriques, D., Pereira, E., Franco, R. J Biotech, 119: p. 111-117.

21. Plech A., Kotaidis, V., Siems A., Sztucki M. Phys Chem Chem Phys, 2008. 10: p. 3888-3894.

22. Cuncheng, L., Shuford, L., Chent, M,., Lee E. J., Cho S. O. ACS Nano, 2008. 2(9): p. 1760-1769.

23. Stichler, C., *Texas alfalfa production*, T.A.E. Service, Editor. 1997, Texas A&M University System.

24. Smartt, J., Simmonds, N. *Evolution of Crop Plants*.1995, New York: John Wiley and Sons.

25. Stochmal, A., Piacente, S., Pizza, C., De Riccardis, F., Leitz, R., Oleszek, W. J Agric Food Chem, 2001. 49: p. 753-758.

26. Dien, B.S., Jung, H., Joachim, G., Vogel, K. P., Castler, M. D., Lamb, J. Biom Bioen, 2006. 30: p. 880-891.

27. Kahkonen, M.P., Hopia, A. I., Vuorela, H. J., Rauhna, J., Pihlaja, K., Kujala, T. S., Heinonen, M. J Agric Food Chem, 1999. 47: p. 3954-3962.

28. Rice-Evans, C.A., Miller, N. J., Bolwell, P. G., Pridham, J. B, Free Rad Res, 1995. 22(4): p. 375-383.

29. USEPA. *Introduction to the concept of green chemistry*. 2008 June 24, 2008; Available from: http://www.epa.gov/greenchemistry/pubs.about_gc.html.

30. Chen, K., Wang, C., Ma, D., Huang W., Bao, X, Chem Comm, 2008: p. 2765.

31. Kerton, F.M., *Alternative solvents for green chemistry*. RSC Green Chemistry, ed. J.H. Clark. Vol. 23-40. 2009, Cambridge: The Royal Society of Chemistry.

32. Gardea-Torresdey, J.L., Parsons, J. G., Gomez, E., Peralta-Videa, J. R., Troiani, H., Santiagi, P., Jose-Yacaman, M, Nano Lett, 2002. 2(4): p. 397-401.

33. Shankar, S.S., Rai, A., Balaprasad, A., Singh, A., Ahmad, A., Sastry, M. Nat Mat, 2004. 3: p. 482-488.

34. Shankar, S.S., Ahmad, A., Pasricha, R., Sastry, M. J Mater Chem, 2003. 13: p. 1822-1826.

35. Gardea-Torresdey, J.L., Tiemman, K. J., Gamez, G., Dokken, K., Tehuacanero, S., Jose-Yacaman, M. J Nanopart Res, 1999. 1(3): p. 397-404.

36. Gardea-Torresdey, J.L., Peralta-Videa, J. R., Parsons, J. G., Mohgalaka, N, S, De la Rosa, G. In: *Metal Nanoclusters in Catalysis and Materials Science: The Issue of Size Control*. B. Corain, Schmid, G., Toshima, N, Editor. 2008, Elsevier. p. 401-411.

37. Armendariz, V., Parsons, J. G., Lopez, M. L., Peralta-Videa, J. L., Jose-Yacaman, M., Gardea-Torresdey, J. L. Nanotechnol, 2009. 20.

38. Armendariz, V., *Bioreduction of gold(III) to gold (I) and nanoparticle formation by oat and wheat biomases in chemistry*, in *Chemistry*. Masters Thesis. 2005, University of Texas at El Paso: El Paso.

39. Mohanpuria, P., Rana, N. K., Yadav, S. K. J Nanopart Res, 2008. 10: p. 507-517.

40. Narayanan, K., Badri, Sakthivel N. Mat Lett, 2008. 62: p. 4588-4590.

41. Parsons, J.G., Peralta-Videa, J. R., Gardea-Torresdey, J. L. in *Developments in Environmental Science*, D. Sarkar, Datta, R., Hannigan, R, Editor. 2007, Elsevier. p. 463-486.

42. Sharma, N.C., Sahi, S. V., Nath, S., Parsons, J. G., Gardea-Torresdey, J. L., Pal, T. Environ Sci Technol, 2007. 41(14): p. 5137-5142.

43. Gamez, G., Gardea-Torresdey, J. L.Adv Environm Res, 2003. 7: p. 563-571.

44. *ASM Handbook. Materials Characterization, K. Mills, Editor. 2008, American Society for Metals: U. S. A.*, in *Glossary*. 2008.

45. Skoog, D.A., Holler, F. J., Crouch, S. R, *Principles of Instrumental Analysis*. 6th ed. 2007: Thompson Brooks/Cole.

46. Smith, D.K., *Diffraction methods. Introduction*, in *ASM Handbook. Materials Characterization*, K. Mills, Editor. 2008, American Society for Metals: U. S. A.

47. Suryanarayana, C., Norton, M. G, *X-ray diffraction. A practical approach*. 1998, New York: Plenum Press.

48. Lachance, G. R., Claisse F. *Quantitative X-ray fluorescence analysis, theory and applications*. 1994, West Sussex: John Wiley and Sons.

49. Jenkins, R., *X-ray fluorescence spectrometry*. 1988: Wiley.

50. Goldstein, J., Newbury D., Joy, D., Lyman, C, Echlin P., Lifshin E., Sawyer L., Michael J, *Scanning electron microscopy and x-ray microanalysis*. 3rd ed. 2003, New York: Springer.

51. Shindo Daisuke, O.T., *Analytical electron microscopy for materials science*. 2002, Japan: Springer-Verlag.

52. Kaupp, G., *Atomic force microscopy, scanning near field optical microscopy and nanoscatching, applications to rough and natural surfaces*. Nanoscience and Technology, ed. B.B. P. Avouris, D. Bimberg, K. von Klitzin, H. Sakaki, R. Wiesendanger. 2006, New York: Springer.

53. Ricci Davide, B.P.C., *The basics of atomic force microscopy*. Atomic force microscopy: biomedical methods and applications, ed. B.P. Carlo. Vol. 242. 2004, Genoa: Humana Press.

54. Duthie Gary G., G.P.T., Kyle Janet A M. Proc Nutr Soc, 2003. 62: p. 599-603.

55. Shimmin, R.G., Schoch, Andrew B., Braun, Paul B. Langmuir, 2004. 20: p. 5613-5620.

56. Chon, S.U., Choi, S., Jeng, S., Jang, H., Pyo, B., Kim, S. Crop Prot, 2000. 21: p. 1077-1082.

57. Ascencio, J.A., Perez, M. , Jose-Yacaman, M. Surf Sci, 2000. 447: p. 73-80.

58. Ramezani, N., Ehsanfar, Z., Shamsa, F., Amin, G., Shahverdi, R. R., Monsef E., Hamid R., Shamsaie, A. Z. Naturforsch, 2008. 63(B): p. 903-908.

59. Yacaman, M.J., Heinemann, C,m Yang, c. Y., Poppa, H. J. Cryst. Growth, 1979. 47: p. 187.

60. Baigorri, R., Garcia-Mina, J. M., Aroca, R. F., Alvarez-Puebla, R. A. Chem. Matter, 2008. 20: p. 1516-1521.

61. Lofton, C., Sigmund, W. Adv. Funct. Mater., 2005. 15: p. 1197.

62. Kirkland, A.I., Jefferson, D. A., Duff, D. G., Edwards, P. P., Gameson, I., Johnson, B. F. G., Smith, D. J. Proc R Soc London Ser. A, 1993. 440: p. 589.

63. Germain, V., Jing, L., Ingert, D., Wang, Z. L., Pileni, M. P. J. Phys. Chem. B, 2003. 107: p. 8717.

64. Reyes-Gasga, J., Gomez-Rodriguez, A., Gao, X., Jose-Yacamán, M. Ultramicroscopy, 2008. 108: p. 929.

65. Goy-Lopez, S., Castro, E., Taboada, P., Mosquera, V. Langmuir, 2008. 24: p. 13186.

66. Li, C.C., Cai, W. P., Cao, B. Q., Sun, F. Q., Li, Y., Kan, C. X., Zhang, L. D. Adv Funct Mater, 2006. 16: p. 83.

67. Wang, L., Chen, X., Zhan, J., Chai, Y., Yang, C., Xu, L., Zhuang, W., Jing, B. J Phys Chem B, 2005. 109: p. 3189.

68. Xie, J., Lee, J. Y., Wang, D. I. C., Ting, Y. P. Small, 2007. 3: p. 672.

69. Serapligia, M., J., Cameron, K. D., Stipanovic, A. J., Smart, L. B. Appl Biochem Biotechnol, 2008. 145: p. 3-11.

Vita

Milka Montes earned her Bachelor's of Science Degree in Chemistry from the University of Texas at El Paso in December 2004 with an honor thesis as she was a MARC fellow student. She joined the UTEP graduate school in 2005 pursuing the new doctoral degree in Chemistry. In her first year as a graduate student, she received an internship at the Children's Nutrition Research Center at Baylor University in Houston.

During her graduate studies, Milka Montes has presented her research in several national and international meeting. During the presentation of her research at national meetings; she has received *the Outstanding Research Poster Presentation Award in* the SACNAS National conference in 2006, and the Outstanding Oral Presentation Award in the SACNAS National conference in 2004. Other awards include the Best teacher assistant award given by the American Chemical Society Student Affiliates in 2008. She has published six articles in peer review journals; one of them as first author, and she has submitted two more for publication.

She was awarded the Alliance for Graduate Education and the Professorate Fellowship, the NSF Bridge to the Doctorate Fellowship and the Dodson Dissertation Fellowship. She has also received numerous honors such as being co-chair for the "environmental chemistry" session at the ACS Southwestern Regional Meeting in El Paso in 2009. She was an invited speaker in the Nanotechnology workshop at the University of Puerto Rico, Mayaguez in 2009; and a presenter at the First Joint Advanced Electron Microscopy School for Nanomaterials in Coahuila, MX.

Milka Montes has been accepted to continue her career as a postdoctoral fellow at the University of California Santa Barbara campus as part of the Center for Environmental Implication in Nanotechnology. Her future plans are to pursue a career in academia as a professor and researcher, and her motivation is to increase scientific knowledge and to help women and minority students to accomplish their dreams as scientists.

List of publications and presentations:

Publications

1. **Montes, M. O**., A. Mayoral, F. L. Deepak, J. G. Parsons, J. R. Peralta-Videa, M. José-Yacamán, J. L. Gardea-Torresdey. **(2010)**. Anisotropic gold nanoparticles and gold plates biosynthesis using alfalfa extracts. **Submitted to Journal of Nanoparticle Research.**

2. **Montes-Holguín, M. O**., Peralta-Videa, J. R., Meitzner, G., Martínez-Martínez, A., De la Rosa, G., Castillo-Michel, H., Gardea-Torresdey, J. L. (**2006**). Biochemical and spectroscopic studies of the response of *Convolvulus arvensis* L. to Cr (III) and Cr (VI) stress. **Environmental Toxicology and Chemistry** 25 (1), 220-226.

Presentations

ABSTRACTS: Research Presentations at Regional, National, and International Meetings.

Oral

1. **Milka O. Montes,** Jose R. Peralta-Videa, Jorge L. Gardea-Torresdey. American Chemical Society, 65th Southwest Regional Meeting. El Paso, TX, November 4-7, 2009.

2. **Milka O**. **Montes.** Formation of Gold Nanoparticles Using Alfalfa Plant Extracts. SACNAS National Conference, Dallas, TX, October 15-18, 2009.

3. **Milka O. Montes**. Nanoparticles in the Environment. Nanotechnology Workshop, University of Puerto Rico-Mayagüez. Mayagüez, Puerto Rico, August 2-6, 2009.

4. **Milka O**. **Montes.** Green Synthesis and Extraction of Gold Nanoparticles Using Alfalfa Biomass. SACNAS National Conference, Salt Lake, UT. October 9-12, 2008.

5. Dokken, K.M., **Montes-Holguin, M.O**., Peralta-Videa, J.R., Gardea-Torresdey, J.L. 2007. Using Infrared Imaging to Determine Changes in Plant Structure Due to Chromium (VI) Exposure. 233rd ACS National Meeting, Chicago, IL, March 25-29, 2007.

6. **Milka O. Montes-Holguin**, Jose R. Peralta-Videa, Michael A. Grusak, Jorge L. Gardea-Torresdey, Spectroscopic studies of Cr(VI) absorption and reduction by *Convolvulus arvensis* and *Medicago truncatula*. 233rd American Chemical Society National Meeting, Division of Chemistry. Chicago, IL. March 25-29, 2007.

7. **Milka O. Montes,** Alejandro Martínez-Martínez, Guadalupe De la Rosa, Hiram A. Castillo-Michel, José R. Peralta-Videa, Jorge L. Gardea-Torresdey, Response to Chromium-induced stress by Convolvulus arvensis L.: Uptake, speciation and enzymatic activity. SACNAS National Conference, Austin, TX 2004.

8. De la Rosa, G., Peralta-Videa, J. R., **Montes, M**., Parsons, J. G., and Gardea-Torresdey, J. L.

2003. Cadmium uptake and translocation in tumbleweed (*Salsola kali*), a potential Cd-hyperaccumulator desert plant species: ICP-OES and XAS studies. 30th Annual SSRL Users' Meeting, Palo Alto, CA, Oct 8-10, 2003.

Poster

1. **Montes, M. O.** Gardea-Torresdey, J. L., Peralta-Videa, J. R., Jose-Yacaman, M. Biosynthesis of Gold Nanoparticles Using Alfalfa Extracts. First Joint Advanced Electron Microscopy School for Nanomaterials and the Workshop on Nanomaterials (AEM-NANOMAT'09). Saltillo, Coahuila, Mexico. September 28-October 1, 2009.

2. **Montes M. O**., Grusak, M. A., Parsons, J.G., Peralta-Videa, J. R., Gardea-Torresdey, J. L. Study of the effect of chromium exposure on sulfur metabolic pathways in the model plant *Medicago truncatula.* 2006 SACNAS National Conference, Tampa, FL. October 2006.

3. **Montes, M.O**., Peralta-Videa, J.R., Gardea-Torresdey, J.L**.** Convolvulus Arvensis L: A Potential Phytoremediator of Cadmium, Chromium and Copper Contaminated Sites. ***2004 Student Research Expo "envision the future".*** The University of Texas at El Paso, El Paso, TX, April 19, **2004.**

4. De la Rosa, G., Gardea-Torresdey, J.L**.**, Aldrich, M.V., **Montes, M.O**. and Peralta-Videa, J.R., Agar and Hydroponics Studies on Pb (II) Absorption by Tumbleweed (Salsola kali): Effect of EDTA on Pb (II) Uptake and Translocation. 2003, SACNAS Conference, Albuquerque, NM, Oct 2-5, **2003**.

5. **Montes, M**., Peralta-Videa, J.R., Gardea-Torresdey, J.L., de la Rosa, G. Convolvulus arvensis L.: a potential phytoremediator of cadmium, chromium, and copper contaminates sites. 227th American Chemical Society National Meeting, Division of Environmental Chemistry. Anaheim, CA, March 28- April 1, **2004.**

6. De la Rosa, G., Peralta-Videa, J. R., **Montes, M.,** Parsons, J. G., and Gardea-Torresdey, J. L. 2003. Cadmium uptake and translocation in tumbleweed (*Salsola kali*), a potential Cd-hyperaccumulator desert plant species: ICP-OES and XAS studies. 30th Annual SSRL Users' Meeting, Palo Alto, CA, Oct 8-10, 2003 (**Invited Talk**)

7. De la Rosa, G., Gardea-Torresdey, J.L., Aldrich, M.V**., Montes, M.O**. and Peralta-Videa, J.R., Agar and Hydroponics Studies on Pb (II) Absorption by Tumbleweed (Salsola kali): Effect of EDTA on Pb (II) Uptake and Translocation. 2003, SACNAS Conference, Albuquerque, NM, Oct 2-5, **2003**.

8. **Montes, M. O.,** Gardea-Torresdey, J.L., Peralta-Videa, J.R., De la Rosa, G., Diaz, B.C. *Convolvulus arvensis* A Potential Phytoremediator for Chromium Contaminated Soils. 2003 SACNAS Conference, Albuquerque, NM, Oct 2-5, **2003**.

9. De la Rosa, G., Gardea-Torresdey, J. L., Peralta-Videa, J. R., Parsons, J. G., **Montes, M.** Potential Cd hyperaccumulation by tumbleweed: ICP-OES and XAS studies. **2003**. Student Research Expo. University of Texas at El Paso **April 17, 2003**.

10. **Montes, M. O.,** Gardea-Torresdey, J. L., Peralta-Videa, J. R., De la Rosa G. Use of *Convolvulus arvensis* L. To phytoextract cadmium, chromium and copper. **2003**. Student Research Expo. University of Texas at El Paso **April 17, 2003**.

11. **Montes, M. O.,** Gardea-Torresdey, J. L., Peralta-Videa, J. R., De la Rosa G. Use of *Convolvulus arvensis* L. To phytoextract cadmium, chromium and copper. **2003**. International Symposium on Applied Bioinorganic Chemistry. University of Guanajuato, April 1-5, 2003.

12. Guadalupe de la Rosa, Jorge L. Gardea-Torresdey, José R. Peralta-Videa, Jason G. Parsons, **Milka Montes**. Potential Cd Hyperaccumulation by tumbleweed: ICP-OES and XAS studies. **2003**. International Symposium on Applied Bioinorganic Chemistry. University of Guanajuato, Guanajuato, Gto., Mexico. April 1-5, 2003.

13. De la Rosa, G; Gardea-Torresdey, J.L.; Peralta-Videa, J.R.; Parsons, J.G.; **Montes, M.** ICP-OES and XAS studies of the Cd uptake by tumbleweed. 225th American Chemical Society National Meeting, Division of Environmental Chemistry. New Orleans, LA, March 23-27, 2003.

Permanent address: 19201 Jay R Vargas

El Paso, TX, 79938

This thesis/dissertation was typed by Milka O. Montes